[Dissertations & Theses (Open Access)](https://digitalcommons.library.tmc.edu/uthson_etd)   Cizik School of Nursing

Spring 5-5-2023

Endothelial To Mesenchymal Transition In Human And Murine Congenital Diaphragmatic Hernia Pulmonary Hypertension

Jamie L. Gilley
UTHealth School of Nursing

Follow this and additional works at: https://digitalcommons.library.tmc.edu/uthson_etd

Part of the Nursing Commons

THE TMC LIBRARY
Health Sciences Resource Center

ENDOTHELIAL TO MESENCHYMAL TRANSITION IN HUMAN AND MURINE

CONGENITAL DIAPHRAGMATIC HERNIA PULMONARY HYPERTENSION

_____

A DISSERTATION

SUBMITTED IN PARTIAL FULFILLMENT OF THE REQUIREMENTS

FOR THE DEGREE OF DOCTOR OF PHILOPSOPHY IN NURSING

THE UNIVERSITY OF TEXAS HEALTH SCIENCE CENTER AT HOUSTON

CIZIK SCHOOL OF NURSING

BY

JAMIE LYNN GILLEY APRN, MSN, NNP-BC

_____

MAY 2023

UTHealth | Cizik

The University of Texas
Health Science Center at Houston | School of Nursing

April 5th, 2023
Date

To the Dean of the Cizik School of Nursing:

I am submitting a dissertation written by Jamie Gilley and entitled "Endothelial to Mesenchymal Transition in Human and Murine Congenital Diaphragmatic Hernia Pulmonary Hypertension." I have examined the final copy of this dissertation for form and content and recommend that it be accepted in partial fulfillment of the requirements for the degree of Doctor of Philosophy in Nursing.

Dr. Sandra K. Hanneman, Committee Chair

We have read this dissertation
and recommend its acceptance:

Sundeep G. Keswani, MD, FACS, FAAP

Madelene J. Ottosen, PhD, RN

Binoy Shivanna, MD, DM, PhD

Accepted,

Dean of the Cizik School of Nursing

Acknowledgements

I would like to express my sincere appreciation to Dr. Sandra K. Hanneman for her time, knowledge, patience, and mentorship throughout my time in the PhD program. I would also like to acknowledge and thank the Laboratory for Regenerative Tissue Repair at Baylor College of Medicine including Dr. Sundeep Keswani, Dr. Swathi Balaji, and Dr. Hui Li, for their guidance and allowing me to utilize their laboratory to complete my dissertation work.

Jamie Gilley

Endothelial to Mesenchymal Transition in Human and Murine Congenital Diaphragmatic Hernia Pulmonary Hypertension

May 2023

Abstract

Background: Congenital diaphragmatic hernia (CDH) is one of the most complex congenital disorders, characterized by pulmonary hypertension and hypoplasia. CDH-associated pulmonary hypertension (CDH-PH) features devastating morbidity and mortality (25-30%) among neonates. An unmet need is determining the mechanisms triggering CDH-PH to save infants and improve their quality of life. Prior data suggest abnormal remodeling of the pulmonary vascular extracellular matrix, presumed to be driven by endothelial-to-mesenchymal transition (EndoMT), hinders postnatal vasodilation and limits efficacy of anti-PH therapy in CDH. Although abnormal vascular development and remodeling are known CDH traits, there is limited data on the role of EndoMT in CDH-PH.

Objective: The purpose of the study was to investigate how EndoMT contributes to CDH-PH by identifying cells undergoing EndoMT as noted by alpha smooth muscle actin (α-SMA) and CD31 expression in human umbilical vein endothelial cells (HUVECs), and lung tissue obtained from murine pups using the nitrofen model.

Methods: CDH (n=8) and control HUVECs (n=8) were stained for α-SMA and CD31 after being exposed for 24hrs to TGF-β, a known EndoMT promoter. Nitrofen (n=8) and control murine (n=8) pup lungs were also stained for α-SMA and CD31. Expressions of α-SMA and CD31 were quantified in the HUVEC, and murine tissue using Fiji imaging software and normalized to the total number of cells per slide noted by DAPI staining.

Results: CDH HUVECs demonstrated a 1.1-fold increase in α-SMA expression (p= 0.02). The murine model did not show statistical significance between nitrofen and

control pup lungs: however, there was a 0.4-fold increase in α-SMA expression with a 0.8-fold decrease in CD31 expression in the nitrofen pup lungs when compared to controls.

Conclusion: These results suggested EndoMT could potentially play a role, albeit modest, in the ECM remodeling seen in CDH-PH.

TABLE OF CONTENTS

Summary of Study

This dissertation encompasses the research proposal that was approved by the Dissertation Committee in May 2022. The manuscript, "*Endothelial to Mesenchymal Transition in Human and Murine Models of Congenital Diaphragmatic Hernia,*" contains the findings of the study to be published for global knowledge. The standardized protocols utilized to complete the research are listed in the appendixes. Also included in the appendixes are the Institutional Review Board (IRB) approvals and the student's curriculum vitae.

The study evaluated the potential role of endothelial-to-mesenchymal transition (EndoMT) as a major driver of congenital diaphragmatic hernia pulmonary hypertension (CDH-PH) pathogenesis. CDH-PH is a leading cause of long-term morbidity, has a 25-30% mortality rate in the neonatal period, and is often refractory to frontline anti-PH therapy. The study investigated how endothelial cells take on a fibroblast-like phenotype to promote pathological remodeling of the vascular extracellular matrix, which ultimately leads to treatment-refractory PH. In the dissertation research, the degree of EndoMT in human umbilical vein endothelial cells (HUVECs) and murine CDH pup lungs was evaluated utilizing the well-established nitrofen murine model for the latter to determine if EndoMT is increased in CDH murine lung tissue and endothelial cells when compared with control samples.

Of note, there was a 6% attrition rate with the control group in the murine model as one mouse did not survive pregnancy due to an unknown medical condition, and one control mouse only had two pups that were excluded from the study due to dysmorphism of unknown etiology, yielding a 6% attrition rate for the murine model. The mice were

replaced by two new female mice of breeding age. Even with replacement, the total number of mice utilized remained within the projected sample size (N=6) for the dams.

Issues were encountered with the initial CD31 rat primary antibody used in the HUVEC model during optimize of the primary and secondary antibody dilutions. Two different staining attempts with the initial CD31 rat primary antibody did not result in the slides being successfully stained despite using a 1:100 and 1:50 dilution. The primary CD31 antibody was switched to rabbit which resulted in a successful fluorescent stain using a 1:100 dilution. The rat primary antibody manufacturer was contacted regarding the staining issues.

The impact of elevated EndoMT in HUVEC and murine CDH models, compared with controls, would validate that CDH endothelial cells take on a fibroblast phenotype that can lead to ECM thickening, which would be a novel finding that could help future researchers investigating CDH-PH pathobiology.

The dissertation research raised several important questions to consider for future researchers. Are there species differences in expression of EndoMT biomarkers, which was suggested by the significant findings in the HUVEC model when compared to the nitrofen model. Is the nitrofen model valid for measuring EndoMT biomarkers; reasons why it may not be valid are discussed in the manuscript under discussion section. Questions also arose regarding the relationship between CDH-PH severity and biomarker expression, which may be suggested by the wide range of expression of α-SMA and CD31 in the present study findings even within species.

ENDOTHELIAL TO MESENCHYMAL TRANSITION IN HUMAN AND MURINE

CONGENITAL DIAPHRAGMATIC HERNIA PULMONARY HYPERTENSION

_____

A DISSERTATION PROPOSAL

SUBMITTED IN PARTIAL FULFILLMENT OF THE REQUIREMENTS

FOR THE DEGREE OF DOCTOR OF PHILOPSOPHY IN NURSING

THE UNIVERSITY OF TEXAS HEALTH SCIENCE CENTER AT HOUSTON

CIZIK SCHOOL OF NURSING

BY

JAMIE LYNN GILLEY APRN, MSN, NNP-BC

_____

JUNE 2022

Specific Aims

Every 10 minutes in the United States, a baby is born with congenital diaphragmatic hernia (CDH) according to Shanmugam, et al. (2017). The incidence of CDH is estimated at 1 per 2,000 to 5,000 births (AlFaleh, et al, 2006). CDH is an anatomic defect where the diaphragm fails to form completely and allows abdominal viscera to herniate into the thorax. CDH is a complex disease with multifactorial pathology and high morbidity and mortality of 25-30% during the neonatal period (Gupta & Harting, 2020); morbidity and mortality largely result from the pulmonary hypertension (PH) and lung hypoplasia that are characteristic of CDH. PH is defined as sustained, supra-normal pulmonary arterial pressure that creates dysfunctional pulmonary circulation and suboptimal gas exchange with subsequent decreased oxygenation, ventilation, and/or cardiac function (Gupta & Harting, 2020). Patients with CDH have structurally and functionally abnormal pulmonary vessels which may contribute to PH in this population (Mous, et al., 2017). Despite clinical advances in therapy, pulmonary hypertension secondary to CDH (CDH-PH) remains a major medical challenge in the management of patients with CDH.

Research shows extracellular matrix (ECM) thickening in the CDH pulmonary vasculature (Monroe, et al., 2020). Thickening of the media and adventitia of pulmonary arteries (Yamataka, et al., 1997) creates a stiff ECM in CDH which decreases luminal diameter, increases resistance to blood flow, and decreases vascular compliance. *Therefore, a stiff pulmonary vascular ECM causes the pulmonary vessel to become a "lead pipe," reducing blood flow and responsiveness to anti-PH therapies.* A major gap in knowledge is the nascence of the science on molecular drivers that promote pathogenic ECM remodeling in CDH-PH**.** One pathway of interest is endothelial-to-mesenchymal transition (EndoMT), which can promote abnormal pulmonary vascular ECM remodeling

and drive PH in multiple adult and pediatric PH diseases; however, EndoMT has not been studied in CDH-PH (Li, et al., 2018). The lack of EndoMT research in CDH-PH is likely due to difficulties in obtaining CDH lung tissue to study endothelial cells.

The goal of the proposed dissertation is to improve global knowledge of a potential underlying mechanism, EndoMT, that could be contributing to the ECM thickening seen in CDH-PH. The *overarching hypothesis is that EndoMT is increased in CDH lung tissue and endothelial cells when compared to controls.* To obtain experimental evidence supporting this hypothesis, the following aims are proposed:

Aim 1: To confirm the presence and estimate the magnitude of EndoMT in CDH and control human umbilical vein endothelial cells (HUVECs) as an ex vivo surrogate to lung tissue.

Hypothesis: CDH HUVECs have at least a threefold increase in EndoMT compared with control samples.

Approach: Compare gestational age-matched controls against CDH HUVECs (n=8 CDH group; n=8 control group) and assess their spatiotemporal expression of EndoMT markers α-SMA and CD31 by immunofluorescence after 24-h exposure to TGF-β, which is known to promote EndoMT (Hashimoto, 2010). Scientific significance will be noted by a threefold or greater increase in α-SMA with a onefold or greater decrease in CD31 expression in CDH samples versus controls.

Aim 2: To investigate the extent of EndoMT in CDH lungs using a nitrofen murine model.

Hypothesis: EndoMT presence in lung tissue is at least threefold greater in mice with an induced CDH phenotype when compared to controls.

Approach: Compare the extent of EndoMT expression in CDH lung samples (n=8) from the nitrofen murine model with EndoMT expression in healthy, age-matched,

murine lung controls (n=8) by examining the spatiotemporal expression of EndoMT markers α-SMA and CD31. EndoMT will be evaluated by immunohistochemistry staining of murine lung tissue. Scientific significance will be noted by a threefold or greater increase in α-SMA with a onefold or greater decrease in CD31 expression in CDH samples versus controls.

Overall Impact

The proposed research plan has been designed to investigate a potential role of EndoMT in CDH-PH. The use of HUVECs will be applied as an ex vivo surrogate model to lung tissue to strengthen the hypothesis that EndoMT plays a role in ECM thickening that contributes to worsening morbidity and mortality from PH in neonates with CDH-PH. Elevated EndoMT in HUVEC and murine CDH models, compared with controls, would validate that CDH endothelial cells take on a fibroblast phenotype that leads to ECM thickening, which would be a novel finding that could help future researchers investigating CDH-PH pathobiology.

Currently, no known marker predicts how severe CDH-PH will be postnatally in infants with CDH; consequently, infants with CDH are managed similarly after birth. CDH-PH severity is determined postnatally by evidence of PH on echocardiography and the need for PH medications. Postnatal management of PH could be tailored to the individual infant if biomarkers are shown to reflect severity of CDH-PH. Future research would benefit from investigating the magnitude of correlation between EndoMT expression and severity of CDH-PH. If a link is established that elevated EndoMT expression is associated with more severe PH, individual care plans could be created to guide postnatal PH treatment.

Background and Significance

EndoMT features a progressive loss of the native endothelial cell (EC) markers and acquisition of a mesenchymal cell phenotype by the production of a fibrotic ECM. During EndoMT, endothelial cells differentiate into mesenchymal-like cells characterized by induced α-SMA expression with a loss of endothelial cell markers and increased collagen deposition (Spillman, et al., 2015). With EndoMT, there is downregulation of the endothelial-specific marker CD31, and upregulation of mesenchymal marker α-SMA (Zhang, et al., 2016). Abnormal vascular development and ECM remodeling are CDH traits, but compelling data that decipher that EndoMT mechanistically contributes to CDH-PH have not yet been obtained.

A critical barrier to advances in CDH-PH research is the lack of human models to study. Prior research has shown that HUVECs can serve as a surrogate for study of pulmonary vascular endothelial biology in various pathologies; preliminary data show that HUVECs reflect what is observed histologically in human CDH tissues (Baudin, et al., 2007). HUVEC-based models have been used since the 1970s as a method to study vascular endothelium properties in conjunction with molecular mechanisms involved in endothelial cell function (Baudin, et al, 2007).

Of the several candidate animal models that characterize cellular transition and mirror human CDH-PH, the nitrofen-induced murine CDH model has minimal complexity and high feasibility and reproducibility (Wild, et al, 2017). Use of this murine model is proposed to complement the HUVEC model to investigate EndoMT in CDH-PH.

Preliminary Data

To investigate how EndoMT contributes to CDH-PH, the student previously conducted experiments for her PhD coursework in human CDH tissue specimens to assess the loss of endothelial lineage markers and reciprocal acquisition of mesenchymal identifiers. Immunohistochemistry performed on lung tissue sections

obtained postmortem from neonates with CDH and stored in the laboratory's biobank revealed an increase in several transitioning cells as indicated by α-SMA⁺ double-positive staining in CDH vessel walls, a potential precursor to fibrosis, when compared to age-matched control samples. Postmortem human CDH lung tissue vessels were isolated by laser capture microdissection to perform proteomics profiling analyses and assess CDH-PH vascular-specific changes, which robustly revealed 53 proteins associated with ECM remodeling, supporting the hypothesis that EndoMT is involved in vascular dysfunction during CDH-PH development. In Aim 2, the researcher will examine murine CDH lung tissue samples to measure the magnitude of EndoMT burden when compared to murine healthy control samples.

HUVECs isolated from umbilical veins at the time of birth will be used as surrogates for endothelial cells because they provide an abundant supply and can be obtained by entirely non-invasive means. This strategy has previously been employed in the study of other lung conditions, including pulmonary fibrosis and environmental injury, where HUVECs have been shown to reflect the behavior of vascular cells in the pulmonary endothelium (Lan, et al., 2020; Williamson, et al., 2016; Saxena, et al., 2021). As proof of concept that a subset of endothelial cells can undergo EndoMT, the student isolated CDH and control HUVECs in the laboratory, treated them with 10 ng/mL of TGF-β for 24 hours, and as expected, observed an increase in EndoMT markers α-SMA (34.0%) with a reciprocal reduction of CD31 (15.3%) in CDH HUVECs compared with control HUVECs. CD31 is reduced with concurrent increases in markers such as α-SMA when cells undergo EndoMT (Good, 2015). Limitations of the preliminary data include the small sample size (n=4/group) due to the unavailability of additional HUVECs at the time of the analysis. Challenges encountered included contamination with the first CDH HUVEC collection resulting in the cells needing to be discarded. The HUVEC isolation

protocol was then modified to include a PBS, alcohol, PBS rinse prior to cell isolation to avoid contamination. Since implementing this additional step, no contamination has occurred. In Aim 1, the student will evaluate CDH HUVEC propensity to undergo EndoMT.

Research Strategy

Mortality in CDH stems from: (i) aberrant development of the lungs, (ii) abdominal viscera invasion into the thoracic compartment through a defective diaphragm, which compresses the affected lung hindering further lung development, and (iii) CDH-PH refractory to PH therapies. While the focus of mainstream research on altered gene expression that contributes to congenital malformation (Kardon, et al., 2017) is important, an immediate challenge confronted at the bedside is severe PH and the survival of neonates with CDH. There is inconsistent effectiveness of frontline anti-PH therapies, including smooth muscle relaxants and vasodilators (Gien, et al, 2016), with some patients being "non-responders" to therapy (Putnam, et al., 2016; Lawrence, et al., 2020). It is estimated that ~75% of infants born with CDH will require treatment for PH; however, the response to treatment varies with no clear estimate of the number and percentage of infants who do not respond (Lawrence, et al, 2020). The high mortality rate secondary to PH in the neonatal period suggests there is a significant number of infants who are non-responders. Thus, it is imperative to study putative mechanisms that may explain the lack of response to PH therapy in order to improve the clinical management of infants with CDH-PH (McCulley, et al, 2018).

Pulmonary arteries in CDH are noted by their thick walls resulting from smooth muscle cell hyperplasia, increased collagen deposition, and marked inflammation that lead to fibrotic perivasculature remodeling (Shah, et al., 2018). Fibroblasts are the primary arbiters of fibrosis in many diseases, including PH; however, whether the fibroblasts responsible for abnormal ECM in CDH-PH are of mesenchymal lineage or

derived from transitioned endothelial cells has not been characterized. The proposed methods are expected to obtain experimental evidence that EndoMT contributes to perivascular ECM thickening in CDH-PH as noted in Aims 1 and 2. During EndoMT, endothelial cells undergo mesenchymal transition, separate from the intimal layer, and migrate into the medial and outer layers to acquire an elongated and fusiform myofibroblast-like morphology with expression of mesenchymal markers (CD31$^-$, vWF$^-$, α-SMA$^+$, Collagen I$^+$) coupled with downregulation of the endothelial-specific marker CD31 (Piera-Velazquez, et al., 2018; Zhang, et al., 2016; Spillman, 2015).

EndoMT leads to pulmonary vascular thickening, and endothelial dysfunction alters downstream signaling pathways, ultimately leading to vascular narrowing and PH (Li, et al., 2018; Good, et al., 2015; Hashimoto, et al., 2010; Stenmark, et al., 2016). CDH-specific animal models also show endothelial dysfunction and impaired vascular growth (Grayck, et al., 2013). Deficient vascular development and ECM thickening are known to occur in CDH; however, little is known about how EndoMT contributes to CDH-PH. It is conceivable that endothelial dysfunction and pathological vascular ECM thickening in CDH-PH is mediated by EndoMT, ultimately causing the lack of responsiveness to PH medications in infants with CDH. During the student's laboratory work, preliminary pre-clinical and clinical data showed increased EndoMT marker gene expression linked to CDH, which prompted the proposed assessment of the extent of EndoMT in the pathological vascular ECM thickening (Aims 1 and 2).

Innovation

This proposal puts forward several new concepts and a new model to investigate putative cellular factors that contribute to CDH-PH. New concepts include the "lead pipe" phenomenon as a major contributor to CDH-PH and EndoMT as a contributing factor to the pulmonary vascular ECM thickening seen in infants with CDH. Comparison of

EndoMT in the pulmonary ECM in CDH versus control endothelial cells (ECs) has not been found in the CDH literature. The utilization of HUVECs as an *ex vivo* model to evaluate EndoMT expression is a novel approach to the study of CDH-PH; no published CDH studies have been located to date that describe the use of HUVECs as a surrogate for lung tissue. Elevated EndoMT expression in HUVECs obtained at birth would suggest that infants with CDH are born with increased EndoMT expression; and, therefore, direct attention to prenatal diagnostic and treatment strategies. Using both a human (HUVEC) model and an animal (murine nitrofen) model permits validation of the findings.

Approach

Aim 1 To confirm the presence and estimate the magnitude of EndoMT in CDH and control HUVECs as an ex vivo surrogate to lung tissue

Hypothesis: CDH HUVECs have at least a threefold increase in EndoMT compared with control samples.

Endothelial dysfunction is a known feature of CDH-PH tissues (Montalva, et al., 2019); differences in the endothelial response seen in CDH secondary to lung hypoplasia and organ compression may be responsible for differences in CDH-PH severity and postnatal treatment response. To address this, HUVECs have been investigated to understand the behavior of pulmonary vascular endothelial cells as a surrogate *ex vivo* model (Medina-Leyte, et al., 2020). Briefly, HUVEC-based models have been used since the 1970s as a method to study vascular endothelium properties in conjunction with molecular mechanisms involved in endothelial cell function (Baudin, et al., 2007; Medina-Leyte, et al., 2020), which helped to glean insight into vascular biology by evaluating different proteins involved in angiogenesis (Medina-Leyte, et al., 2020). HUVECs represent an abundant and non-invasive resource that may

demonstrate endothelial dysfunction in neonates with CDH-PH. This well-established model will be used to study endothelial cell pathophysiology in CDH-PH to help uncover inherent differences in EndoMT expression in healthy controls and patients with CDH-PH.

Gestational age-matched controls will be compared with CDH HUVEC specimens that were previously obtained and are currently stored in the HUVEC biobank at Texas Children's Hospital (n=8/group as noted in Appendix A). HUVECs previously obtained from twin births will be excluded from this study due to lack of generalizability to the CDH population as only six cases of CDH have been documented in twins (Wang, et al., 2015). The student was added to the previously approved Baylor College of Medicine IRB protocol. HUVECs were isolated and stored per HUVEC isolation protocol as part of the student's PhD laboratory coursework (see Appendix D). HUVECs will be cultured and exposed to TGF-β for 24 hours. The spatiotemporal expression of EndoMT markers α-SMA and CD31 will be examined by immunofluorescence (see protocol in Appendix E).

Acceptable reproducibility of Aim 1 analysis and findings will be achieved by utilizing a standardized and documented protocol for immunofluorescence analysis. Previously collected HUVEC samples had endothelial cells isolated using a standardized protocol to decrease variability in EC isolation and enhance reproducibility. All results of the study will be disclosed even if they do not support the proposed hypothesis.

Expected Results 1

Endothelial cells derived from CDH HUVECs will have a greater expression of EndoMT, as measured by mesenchymal marker expression, when compared to controls.

Aim 2 To investigate the extent of EndoMT in CDH lungs using a nitrofen murine model

Hypothesis: EndoMT's presence in lung tissue is threefold greater in mice with an induced CDH phenotype when compared to controls.

A nitrofen-induced mouse model that develops a diaphragmatic defect and lung maldevelopment, like that observed in human CDH, will be used to investigate *in vivo* mechanisms behind CDH-PH. This model, which is widely used in CDH research, shows the expected pulmonary hypoplasia and ECM depostion reflective of human disease. Due to the nearly uniform mortality by postnatal day one, this model will be used to study the early development of CDH-PH and the contribution of EndoMT in its pathogenesis (Chiu, et al., 2014).

A total of 16 lung tissue samples (*n*=8 murine CDH and *n*=8 murine control) will be needed to obtain a medium estimated effect size (Appendix A). Post-mortem lung tissue samples obtained from mice with a nitrofen-induced CDH phenotype per the nitrofen mouse model protocol (see Appendix F) will be evaluated for the extent of EndoMT presence compared with controls. Briefly, CD1 pregnant dams will be gavaged with 100 mg of nitrofen at embryonic day 8.5 (CDH group). Pregnant dams of both the control and CDH group will then undergo C-section at embryonic day 18.5 and pup lungs will be harvested, embedded as whole organ mounts, and placed in paraffin blocks for preservation. When preparing lung tissue samples for assessment, orientation will be controlled by placing the left lung on the left side of the cassette. The paraffin blocks will be sectioned, placed on slides, de-paraffinized, and stained to examine the spatiotemporal expression of EndoMT markers α-SMA and CD31 by immunohistochemistry (see protocol in Appendix G). α-SMA and CD31 co-localization will be evaluated with immunohistochemistry to determine the presence of EndoMT and compared with the control murine lung tissue samples.

Reproducibility of Aim 2 analysis and findings will be achieved by utilizing a

standardized and documented protocol for all murine experiments conducted along with disclosing all results, including those that do not support the hypothesis.

Expected Results 2

A ≥ threefold increase in co-localization of α-SMA and ≥ onefold decrease in CD31 (evidence of EndoMT) in CDH murine lung tissue samples compared with control levels are expected.

Data Analysis

The goal is to detect a difference between control and disease samples. The proposed research plan may serve as a pilot study given the lack of effect size estimates in the literature for α-SMA and CD31 in HUVEC and murine models. A sample size of 8 HUVECs per group (CDH and control) and 8 mice per group (CDH and control) is expected to generate an adequate effect size estimate of difference between CDH and control samples to guide future research with this total accounting for a 20% attrition rate. HUVEC and murine differences will be tested for significance with the 2-tailed independent t-test. A p-value ≤ 0.05 will be considered statistically significant. Statistical analysis will be performed utilizing GraphPad Prism software.

Research Subject Risk and Protection

Approval to conduct the dissertation research will be obtained from both the University of Texas Health Science Center at Houston (UTHealth) and Texas Children's Hospital/Baylor College of Medicine (TCH/BCM) human subject and animal welfare institutional review boards, in compliance with UTHealth policies that govern student research, and after dissertation committee approval of the research plan and before the experiments commence. Policies and requirements of both institutions will be followed.

Vertebrate Animals

Work with mice will be performed at TCH/BCM facilities. The Center for Comparative Medicine (CCM) is responsible for the animal care and use program at TCH/BCM. The CCM maintains full accreditation from the Association for Assessment and Accreditation of Laboratory Animal Care, International (AAALAC) and complies with the U.S. Animal Welfare Regulations, the National Research Council (NRC) Guide for the Care and Use of Laboratory Animals (Guide), and the Public Health Service Policy on the Humane Care and Use of Laboratory Animals (Policy). Animals will be housed in biohazard containment rooms in the small animal facility in the TCH Feigin Center, a full-service facility which also contains surgical suites and autopsy facilities. All animals are observed daily (including weekends) by animal care staff. CCM employs five full-time veterinarians to ensure adequate care of the animals housed within the facility. Animals will be housed five per cage and allowed food and water *ad libitum* in the vivarium.

The UTHealth Animal Welfare Committee (AWC) is responsible for overseeing provisions for the care and well-being of animals used for research and educational purposes at UTHealth and serves the public by ensuring compliance with all legal and ethical standards regarding the use of vertebrate animals in research and teaching. The Center for Laboratory Animal Medicine and Care (CLAMC) is responsible for the health and well-being of laboratory animals used for UTHealth's biomedical research programs. CLAMC provides professional veterinary, surgical, and animal care services, and its staff includes veterinarians, veterinary technicians, and multiple animal care and support personnel. CLAMC also provides training on the care and use of animals for faculty, staff and trainees.

Description of Procedures

To investigate the effects of EndoMT in CDH, CD1 mice of both sexes will be purchased from the BCM core facility. Time-dated pregnant CD1 dams will receive an oral gavage of nitrofen at E8.5 to induce teratogen-associated diaphragmatic hernia. CD1 mice will be used because nitrofen induction of CDH has not been successful with other genetic backgrounds (Wild, 2017). CD1 mice will also be time mated. Preliminary observations at the TCH/BCM laboratory suggest a 20% mortality rate owing to surgical and anesthesia complications, which has been accounted for in the proposed sample sizes. The nitrofen mouse model has a very high mortality in the CDH pups by postnatal day one; therefore, lung removal in the nitrofen model will be completed after C-section or by postnatal day one in the pups after decapitation.

Justifications

Mice are needed for these experiments because there are limited alternative *in vivo* models that incorporate all elements of the mammalian pulmonary system. Too little is known about this system for the development of computer simulations. Mice are a well-accepted model for studying neonatal lung injury. The nitrofen murine model has previously been characterized (Chiu, 2014). Mice and humans share 99% of their individual 30,000 genes suggesting the murine lung model is similar to that of humans (Wild, 2017).

Minimization of Pain and Distress

Animals will be monitored throughout the experiments at 15-minute intervals to assess animal health and pain level. Mice will undergo anesthesia with inhaled isoflurane (1.5–3%) prior to C-section for pup removal. This agent was selected due to its rapid induction, reliable plane of surgical anesthesia, and low complication rate. Mice

will receive buprenorphine (0.05-0.1 mg/kg) administered subcutaneously at time of C-section.

Method of Euthanasia

Mice will be euthanized after C-section by increasing the flow of inhaled isoflurane, accompanied by cervical dislocation. Fetal pups will be euthanized prior to lung removal by decapitation for *ex vivo* analysis.

Human Subjects

Risks to Human Subjects

Using a retrospective case control design, isolated umbilical vein endothelial cells from umbilical cords of mothers of fetuses with a diagnosis of CDH or healthy fetuses (controls) will be used. Mothers were identified and consent obtained at Texas Children's Hospital for participation in studies of EndoMT. At delivery, a sample (5-10 inches) of the discarded umbilical cord was collected in a coded vial by the operative team. Endothelial cells were isolated and will be analyzed for EndoMT expression as part of the proposed dissertation research.

Study Procedures, Materials, and Potential Risks

There is minimal risk to human subjects with the only risk being possible loss of confidentiality.

Adequacy of Protection Against Risks

Due to the minimal risk of loss of confidentiality, all human data from HUVECs will be de-identified to minimize this risk.

Informed Consent and Assent

Not applicable. This study will use specimens previously collected under a different protocol and principal investigator.

Protections Against Risk

There is no risk to subjects.

Vulnerable Subjects

Endothelial cells from umbilical cords of pregnant women will be used for this research study. Informed consent was obtained under a different protocol and principal investigator for umbilical cord collection per Baylor IRB protocol in accordance with HHS 45 CFR Part 46, Subparts B and D.

Potential Benefits of the Proposed Research to Research Participants and Others

There is no direct benefit to individual patients; however, the knowledge gained from the study could inform future interventions to treat PH in neonates with CDH. Because there is no greater than minimal risk to the research subjects and the knowledge gained may lead to reduced morbidity and mortality of neonates with CDH, the risk-benefit ratio is favorable.

Importance of the Knowledge to be Gained

The presence of EndoMT in the setting of CDH may inform future research to develop therapies to attenuate EndoMT and its associated fibrosis in neonates with CDH-PH. Given the minimal risk to the subjects who donated their umbilical cords and

the potential importance of this knowledge to clinical practice, this study has a very

reasonable risk-to-benefit ratio.

Literature Cited

AlFaleh, K., Lee, K. S., Ramsey, J., & Nowaczyk, M. (2006). Genetic considerations in
recurrent congenital diaphragmatic hernia in two siblings. *Annals of Saudi
Medicine, 26(5),* 391–394. doi:10.5144/0256-4947.2006.391

Baudin, B., Bruneel, A., Bosselut, N., & Vaubourdolle, M. (2007). A protocol for isolation
and culture of human umbilical vein endothelial cells. *Nature Protocols, 2,* 481
485. PMID: 17406610

Chiu, P. P. (2014). New Insights into Congenital–Diaphragmatic Hernia - A Surgeon's
Introduction to CDH Animal Models. *Frontiers Pediatrics, 2:36.* PMID: 24809040

Chung, Y. H., et al. (2017). MiR-30a-5p inhibits epithelial-to-mesenchymal transition and
upregulates expression of tight junction protein claudin-5 in human upper tract \
urothelial carcinoma cells. *International Journal Molecular Science,* 18, 1826.
PMID: 28829370

Clipp, R. B., & Steele, B. N. (2009). Impedance boundary conditions for the pulmonary
vasculature including the effects of geometry, compliance, and respiration. *IEEE
Transactions on Biomedical Engineering*, 56, 862–870. PMID: 19068419

Cordier, A.-G., Russo, F. M., Deprest, J., & Benachi, A. (2020). Prenatal diagnosis
imaging, and prognosis in Congenital Diaphragmatic Hernia. *Seminars in
Perinatology, 44,* 51163. PMID: 31439324

Devine, W. P., Wythe, J. D., George, M., Koshiba-Takeuchi, K., & Bruneau, B. G. (2014).
Early patterning and specification of cardiac progenitors in gastrulating mesoderm. *Elife
3,* 508. PMID: 25296024

Evrard, S., et al. (2016). Endothelial to mesenchymal transition is common in atheroscleroticlesions and is associated with plaque instability. *Nature Communications 7,* 11853. https://doi.org/10.1038/ncomms11853

Gien, J., & Kinsella, J. P. (2016). Management of pulmonary hypertension in infants with congenital diaphragmatic hernia. *Journal of Perinatology 36 Supplementary 2,* S28–31. PMID: 27225962

Good, R. B., et al. (2015). Endothelial to mesenchymal transition contributes to endothelial dysfunction in pulmonary arterial hypertension. *The American Journal of Pathology 185,* 1850–1858. PMID: 25956031

Grayck, E., Partrick, D. A., & Gien, J. (2013). Pulmonary artery endothelial cell dysfunction and decreased populations of highly proliferative endothelial cells in experimental congenital diaphragmatic hernia. *American Journal Physiology Lung Cell Molecular Physiology, 305(12):*L943-L952. PMID: 24124189

Gupta, V. S., & Harting, M. T. (2020). Congenital diaphragmatic hernia-associated pulmonary hypertension. *Seminars in Perinatology, 44,* 151167. PMID: 28641752

Hallgren, K. A. (2012). Computing inter-rater reliability for observational data: an overview and tutorial. *Tutorials In Quantitative Methods For Psychology, 8(1),* 23–34. https://doi.org/10.20982/tqmp.08.1.p023

Hashimoto, N., et al. (2010). Endothelial-mesenchymal transition in bleomycin-induced pulmonary fibrosis. *American Journal of Respiratory Cell and Molecular Biology 43,* 161 172. PMID: 19767450

He, L. et al. (2016). Genetic lineage tracing discloses arteriogenesis as the main

  mechanism for collateral growth in the mouse heart. *Cardiovascular Research,*

  109, 419–430. PMID: 26768261

He, L., Tian, X., Zhang, H., Wythe, J. D. & Zhou, B. (2014). Fabp4-CreER lineage

  tracing reveals two distinctive coronary vascular populations. *Journal of Cellular*

  and Molecular Medicine 18, 2152–2156. PMID: 25265869

Kardon, G. et al. (2017). Congenital diaphragmatic hernias: from genes to mechanisms

  to therapies. *Disease Models & Mechanisms 10,* 955–970. PMID: 28768736

Lally, K. P. & Engle, W. (2008). Postdischarge follow-up of infants with congenital

  diaphragmatic hernia. *Pediatrics, 121,* 627–632. PMID: 18310215

Lan, Y., et al. (2020). Urban PM2.5 reduces angiogenic ability of endothelial cells in an

  alveolar capillary co-culture lung model. *Ecotoxicology Environment Safety,*

  202:110932. PMID: 32800216

Lawrence, K. M., et al. (2020). Inhaled nitric oxide is associated with improved

  oxygenation in a subpopulation of infants with congenital diaphragmatic hernia

  pulmonary hypertension. *Journal of Pediatrics, 219,* 167–172. PMID: 31706636

Li, Y., Lui, K. O. & Zhou, B. (2018). Reassessing endothelial-to-mesenchymal transition

  in cardiovascular diseases. *Nature Reviews Cardiology, 146,* 873. PMID:

  29748594

Liu, Q., et al. (2015). Genetic targeting of sprouting angiogenesis using Apln-CreER.

  Nature Communications, 6, 6020. PMID: 2559728

Liu, Q., et al. (2016). Smooth muscle origin of postnatal 2nd CVP is pre-determined in

 early embryo. *Biochemical And Biophysical Research Communications, 471,*

 430–436. PMID: 2690211

Lizama, C. O., et al. (2015). Repression of arterial genes in hemogenic endothelium is

 sufficient for haematopoietic fate acquisition. *Nature Communications, 6,* 7739.

 PMID: 26204127

Ma, W., McKeller, M.R., Rangel, R., Ortiz-Quintero, B., Blackburn, M.R., & Martinez

 Valdez, H. (2012). Spare PRELI gene loci: failsafe chromosome insurance. *PLoS*

 *One. 7(5):*e37949. PMID: 22666421

Madenci, A. L., et al. (2013). Another dimension to survival: predicting outcomes with

 fetal MRI versus prenatal ultrasound in patients with congenital diaphragmatic

 hernia. *Journal Pediatric Surgery, 48(6):*1190-1197. PMID: 23845606

Madisen, L., et al. (2010). A robust and high-throughput Cre reporting and

 characterization system for the whole mouse brain. *Nature Neuroscience, 13,*

 133–140. PMID: 20023653

McCulley, D. J., et al. (2018). PBX transcription factors drive pulmonary vascular

 adaptation to   birth. *Journal of Clinical Investigation, 128,* 655–667. PMID:

 29251627

McLeod, S. A., 2019. What does effect size tell you. *Simply Psychology:*

 https://www.simplypsychology.org/effect-size.html

Medina-Leyte, D.J., Domínguez-Pérez, M., Mercado, I., Villarreal-Molina, M.T., & Jacobo
Albavera, L. (2020). Use of human umbilical vein endothelial cells (HUVEC) as a
model to study cardiovascular disease: A Review. *Applied Sciences, 10(3):*938.
https://doi.org/10.3390/app10030938

Monroe, M.N., et al. (2020). Extracellular vesicles influence the pulmonary arterial
extracellular   matrix in congenital diaphragmatic hernia. *Pediatric Pulmonology,
55(9):*2402-2411. PMID: 32568428

Montalva, L., Antounians, P. H. L. & Zani, A. (2019). Pulmonary hypertension secondary
to congenital diaphragmatic hernia: factors and pathways involved in pulmonary
vascular remodeling. *Pediatric Research, 85*, 754–768. PMID: 30780153

Mous, D. S., Buscop-van Kempen, M. J., Wijnen, R., Tibboel, D., & Rottier, R. J. (2017).
Changes in congenital diaphragmatic hernia associated PH explain
unresponsiveness to pharmacotherapy. *Respiratory Research, 18(1),* 187.
doi:10.1186/s12931-0170670-2

Pairwise Comparison Post Hoc Tests for Critical Values of Mean Differences. (2021,
July 14). Taft College. https://stats.libretexts.org/@go/page/17385. Retrieved
January 6th, 2022.

Piera-Velazquez, S., Mendoza, F. A. & Jimenez, S. A. (2016). Endothelial to
mesenchymal transition (EndoMT) in the pathogenesis of human fibrotic
diseases. *Journal Clincal Medicine, 5,* 45. PMID: 27077889

Putnam, L. R. et al. (2016). Evaluation of variability in inhaled nitric oxide use and
    pulmonary hypertension in patients with congenital diaphragmatic hernia. *JAMA
    Pediatrics, 170,* 1188–1194. PMID: 27723858

Ranchoux, B., et al. (2015). Endothelial-to-mesenchymal transition in pulmonary
    hypertension. *Circulation. 131(11)*:1006-1018. PMID: 25593290

Russo, et al.(2017). Lung size and liver herniation predict need for extracorporeal
    membrane oxygenation but not pulmonary hypertension in isolated congenital
    diaphragmatic hernia: systematic review and meta- analysis. *Ultrasounds in
    Obstetrics and Gynecology, 49(6):*704 713. PMID: 27312047

Saxena, A., et al. (2021). Extracellular vesicles from human airway basal cells respond
    to cigarette smoke extract and affect vascular endothelial cells. *Scientific
    Reports, 11(1):*6104. PMID:33731767

Shah, M., Phillips, M.R., Quintana, M., Stupp, G., & McLean, S.E. (2018).
    Echocardiography allows for analysis of pulmonary arterial flow in mice with
    congenital diaphragmatic hernia. *Journal Surgical Research, 221,* 35-42. PMID:
    29229150

Shanmugam, H., Brunelli, L., Botto, L. D., Krikov, S., & Feldkamp, M. L. (2017).
    Epidemiology and prognosis of congenital diaphragmatic hernia: a population
    based cohort study in Utah. *Birth Defects Research.* doi: 10.1002/bdr2.1106

Spillman, F., Miteva, K., Pieske, B., Tschope, C., & Van Linthout, S. (2015). High density
    lipoproteins reduce endothelial to mesenchymal transition. *American Heart
    Association.* DOI: 10.1161/ATVBAHA.115.305887

Stenmark, K. R., Frid, M. & Perros, F. (2016). Endothelial-to-mesenchymal transition: an evolving paradigm and a promising therapeutic target in pulmonary arterial hypertension. *Circulation, 133,* 1734 1737. PMID: 27045137

Style, C. C. et al. (2020). Accuracy of prenatal and postnatal imaging for management of congenital lung malformations. *Journal Pediatric Surgery, 55,* 844–847. PMID: 32087934

Style, C. C. et al. (2019). Early vs late resection of asymptomatic congenital lung malformations. *Journal Pediatric Surgery, 54,* 70-74 (2019). PMID: 30366720

Style, C. C. et al. (2019). Fetal endoscopic tracheal occlusion reduces pulmonary hypertension   in severe congenital diaphragmatic hernia. *Ultrasound Obstetric Gynecology, 54,* 752   758. PMID: 30640410

Wang, Y. et al. (2010). Ephrin-B2 controls VEGF-induced angiogenesis and lymphangiogenesis. *Nature, 465,* 483–486. PMID: 20445537

Wang, W., Pan, W., Chen, J., Xie, W., Liu, M., & Wang J. (2015). Outcomes of congenital diaphragmatic hernia in one of the twins. *American Journal of Perinatology, 3,* 114-116.

Wild, B., St-Pierre, M.E., Langlois, S., & Cowan, K.N. (2017). Elastase and matrix metalloproteinase activities are associated with pulmonary vascular disease in the nitrofen rat model of congenital diaphragmatic hernia. *Journal Pediatric Surgery, 52(5):*693-701. PMID: 28189447

Williamson, J.D., Sadofsky, L.R., Crooks, M.G., Greenman, J., & Hart, S.P. (2016).
Bleomycin increases neutrophil adhesion to human vascular endothelial cells
independently of upregulation of ICAM-1 and E-selectin. *Experimental Lung]*
*Research, 42(8-10):*397-407. PMID: 27797602

Yamataka, T., & Puri, P. (1997). Pulmonary artery structural changes in pulmonary
hypertension complicating congenital diaphragmatic hernia. *Journal Pediatric*
*Surgery, 32(3):*387-390. PMID: 9093999

Zhang, Y., et al. (2016). Endothelial to mesenchymal transition contributes to arsenic
trioxideinduced cardiac fibrosis. *Scientific Report, 6,* 33787.
https://doi.org/10.1038/srep33787

Zhou, Q., Yang, M., Lan, H. & Yu, X. (2013). MiR-30a negatively regulates TGF-β1
induced epithelial- mesenchymal transition and peritoneal fibrosis by targeting
Snai1. The American Journal of Pathology, 183, 808–819. PMID: 238313

Appendix A

Sample Size Estimation for Aim 1 and Aim 2 of the Proposed Research Plan

Appendix A

Sample Size Estimation for Aim 1 and Aim 2 of the Proposed Research Plan

The literature was examined for sample size justification in experiments studying

EndoMT in HUVEC and murine models; no study was located that reported α-SMA or

CD31 expression in a HUVEC or murine model that could be used to estimate sample

sizes for the proposed study. An effect size was hypothesized on a theoretical basis and

data from a non-CDH-PH population that showed a three- to six-fold increase in EndoMT

marker α-SMA (Evrard, et al., 2016). A post-hoc power analysis will be done at the end

of the study if the effect size is less than hypothesized, and the study findings will be

reported as pilot data that can be used to estimate effect sizes for future research. To

estimate the sample size for the study, G*Power was utilized with the parameters: *t*-test,

two independent groups, Cohen's d of 2 indicating the group means differ by two

standard deviations (McLeod, 2019), power ≥ .80, α ≤ .05, two-tailed.

t tests - Means: Difference between two independent means (two groups)

Analysis:	A priori: Compute required sample size		
Input:	Tail(s)	=	Two
	Effect size d	=	2
	α err prob	=	0.05
	Power (1-β err prob)	=	0.8
	Allocation ratio N2/N1	=	1
Output:	Noncentrality parameter δ	=	3.4641016
	Critical t	=	2.2281389
	Df	=	10
	Sample size group 1	=	6
	Sample size group 2	=	6
	Total sample size	=	12
	Actual power	=	0.8764178

Based on the estimated sample size and accounting for a 20% attrition rate, 16 samples

per aim (a total of 8 samples will be needed for each CDH and control group in the

HUVEC and murine models).

Appendix B

HUVEC Isolation Protocol

Appendix B

HUVEC Isolation Protocol

The HUVEC Isolation Protocol was developed for the Laboratory for Regenerative

Tissue Repair at Texas Children's Hospital and Baylor College of Medicine using

HUVECs previously isolated as part of PhD coursework by Jamie Gilley, APRN, MSN,

NNP-BC; PhD in Nursing Student, UTHealth Houston, Cizik School of Nursing. This

protocol was adapted from the Baudin, et al. protocol on isolating HUVECs (2007).

Materials:

o   200-ml sterile PBS with 1% Penicillin/Streptomycin

o   70% ETOH solution

o   50 ml conical tubes x 4

o   500-ml sterile container

o   PBS solution

o   0.2% Collagenase

o   Endothelial cell medium

o   2 sterile surgical clamps, sterile scissors

o   60-ml syringe, 10-ml syringe

o   Butterfly needle

o   Fibronectin-coated culture dish

Cord Collection:

- Written consent obtained from mother per IRB protocol

- Don nonsterile gloves. In 500-ml sterile container, mix 200-ml sterile PBS with 2 ml of

1% Penicillin/Streptomycin

- Cord collected from delivery and placed into PBS/Penicillin/Streptomycin solution and

brought back to lab for cell culturing.

- If unable to immediately culture cells, the cord + solution can be placed in a refrigerator at less than or equal to 4 degrees for 12 hours

   - Do not store cord for longer than 12 hours to avoid contamination

HUVEC Isolation:

1)   Don nonsterile gloves. Immediately place umbilical cord in 200-ml PBS with 2 ml of 1% Penicillin/Streptomycin in sterile container.

2)   Keeping plastic umbilical clamps in place. Fill two 50 ml conical tubes with 30 mLs PBS and one conical tube with 30 mL of 70% ETOH. Rinse cord with PBS, 70% ETOH, and then again with PBS using a new tube for each rinse.

3)   Remove plastic umbilical clamps by cutting the umbilical cord below the clamp.

4)   Cannulate umbilical vein with butterfly needle (keep plastic needle protector in place).

5)   Clamp umbilical cord with sterile surgical clamps to secure butterfly needle in place.

6)   Rinse vein via catheter with PBS until effluent is clear (normally ~30-40 mL PBS).

7)   Inject with collagenase and clamp distal end of cord with a sterile surgical clamp once the collagenase drips through.

8)   Continue injecting until vein is pressurized with collagenase.

9)   Leave syringe with collagenase in place and incubate cord for 20 min at room temperature.

a)   After 10 minutes, gently massage cord with fingers. Repeat massage at end of incubation time.

10)   Fill a 50-ml conical tube with 10-ml endothelial medium.

11)   Unclamp distal end of cord over conical tube and rinse with 40-ml of sterile PBS.

12)   Pellet cells in centrifuge at room temperature at 700 g-force for 10 minutes.

13)   Aspirate supernatant and resuspend cells in 5 mLs of endothelial medium.

14)   Aspirate cells and plate on fibronectin coated culture dish and place in incubator. Check cells daily, changing medium every 2-3 days as needed.

15)   Once cells have reached confluence (5-7 days), place cells in a 10 mL conical tube and place in -80 freezer. Containers will be labeled based on de-identified CDH or control collection numbers. Ex: CDH 4 or Control 4

Reference

Baudin, B., Bruneel, A., Bosselut, N., & Vaubourdolle, M. (2007). A protocol for
    isolation and culture of human umbilical vein endothelial cells. *Nature
    Protocols*, *2*(3), 481–485. https://doi.org/10.1038/nprot.2007.54

Appendix C

Microscopy Protocol for Evaluation of EndoMT using the Leica DMi 8 750

Appendix C

Microscopy Protocol for Evaluation of EndoMT using the Leica DMi 8 750

Laboratory Equipment and Supplies

- o   Non-sterile gloves

- o   Microscope lens tissue wipes

- o   Empty syringe

- o   Camel hairbrush

- o   Laboratory notebook

- o   Leica DMi 8 microscope and dust cover

- o   Pre-stained alpha smooth muscle actin and CD31 slides from CDH and control subjects in slide box

- o   Space with sufficient lighting

- o   Power outlet with electricity provided

Preparation

1. Follow Good Laboratory Practices (GLP) when handling slides. Wear laboratory coat and non-sterile gloves. Clean up accidental slide breakage with laboratory broom and dustpan while wearing protective clothing and non-sterile gloves. Follow laboratory regulations for disposal of materials.

2. Tissue slide samples should be kept at room temperature during storage and usage.

3. Wash hands.

4. Don non-sterile gloves.

5. Assemble supplies for slide evaluation along with laboratory notebook for documentation.

6. Obtain slide box with pre-stained slides to be evaluated.

7. Go to room where Leica DMi 8 microscope is located and stored. Remove dust cover.

8. Evaluate the microscope to make sure all the microscope components are present and intact. If any optical surfaces become coated with dust or dirt, clean the surface by blowing it off with a syringe filled with air or brushing it off with a camel hairbrush before attempting to wipe the surface clean with a microscope lens wipe.

9. Make sure microscope is plugged in.

10. Turn on microscope. Allow sufficient time for the microscope light to reach full illumination.

11. Evaluate the microscope components and make sure all of them are functioning including the eye cups, light, focusing knob, stage, condenser, and the illumination control knob by starting at the lowest illumination setting then increasing to the highest setting.

Procedure

1. Position a tissue specimen slide on the specimen stage by sliding it under the slide grips.

2. Using the X/Y stage control, position the specimen slide such that a part of the specimen is under the objective used.

3. Rotate the objective nosepiece using the knurled ring in such a way that the objective with the lowest magnification level is rotated into the working position.

4. Move the specimen stage upwards by turning the coarse focusing knob as far as it will go to the maximum position.

5. Look into the eyepieces and adjust the illumination intensity to a level that is comfortable for your eyes.

6. Bring the specimen into focus using the fine focusing knob.

7. Adjust the eye tubes to your interpupillary distance. Fold or unfold the eye tubes to decrease or increase the distance between the eyepieces until you see one illuminated circle.

8. Using the fine focus adjusting knob, focus on the specimen while looking through only one of the eyepieces. To help focus, cover or close the other eye. Then, look with the other eye just through the other eyepiece. Focus the specimen by using the focusing capability in the focusing eyepiece.

9. Grip the knurled ring on the focusing eyepiece with one hand and rotate the top of the eyepiece with the other hand until the specimen is in focus for this eye and this focusing eyepiece. This corrects for any vision differences between your right eye and left eye.

10. Switch to an objective with a high magnification level and bring the microscope into focus while looking through the eyepiece with both eyes.

    a. The higher magnifications have a shallow lower depth of field. Therefore, after focusing with a high magnification, when you change to a lower magnification you will only have to adjust the fine focus slightly, if at all.

11. Evaluate the slide and determine the pulmonary cells.

    a. Once the pulmonary cells have been identified, evaluate the alpha smooth muscle actin and CD31 staining around the pulmonary cells which identifies the extracellular matrix (ECM) of the cells.

    b. Count the total number of endothelial cells, total number of α-SMA and CD31 stained endothelial cells in each slide.

    c. Document the slide number, total number of endothelial cells, and the total number of α-SMA and CD31 stained cells in the laboratory notebook.

12. Once you have completed evaluating the slide, remove the slide from the stage and place it in the slide box. If oil is present on the eye piece lens, a microscope lens tissue wipe may be utilized to clean the lens.

   a. Care must be taken between evaluating the slides to not alter the focus knob. The weighted knob feature helps to decrease any accidental movement.

   b. If focus is altered in any way between slide evaluations, repeat steps 1-12 to bring the object back into focus.

13. After evaluating the slides, turn off the microscope and replace the dust cover.

14. Place slide holder box, microscope lens tissue wipes, syringe, and camel hairbrush back in their correct storage area.

15. Remove nonsterile gloves and dispose in the trash. Wash hands.

References

1. Leica, (2022). Leica DMi 8. Retrieved from https://www.leica microsystems.com/products/light-microscopes/p/leica-dmi8

Research Manuscript for Submission to Karger Neonatology

Endothelial to Mesenchymal Transition in Human and Murine Models of

Congenital Diaphragmatic Hernia

Jamie Gilley[a,b], APRN, MSN, NNP-BC

[a] PhD Program, UTHealth Houston Cizik School of Nursing, Houston, Texas, USA

[b] Department of Neonatology, Texas Children's Hospital, Houston, Texas, USA

Short Title: EndoMT in CDH

Corresponding Author:

Full name: Jamie Gilley

6901 Bertner Ave, Suite 585

Houston, Texas, 77030, USA

Tel: 713-500-2000

E-mail: Jamie.L.Gilley@uth.tmc.edu

Number of Figures: 3 figures

Word count: Abstract (250) and body text (1906)

Max word count: (total 2500 document not including abstract/figures/title page), abstract (250)

Abstract

Congenital diaphragmatic hernia is one of the most complex congenital disorders, characterized by pulmonary hypertension and lung hypoplasia. CDH-associated pulmonary hypertension (CDH-PH) leads to devastating neonatal morbidity and mortality (25-30%). Understanding of mechanism(s) underlying CDH-PH may improve infant survival and quality of life. Prior data suggest abnormal remodeling of the pulmonary vascular extracellular matrix (ECM), presumed to be driven by endothelial-to-mesenchymal transition (EndoMT), hinders postnatal vasodilation and limits efficacy of anti-PH therapy in CDH. EndoMT is characterized by progressive loss of endothelial markers on native endothelial cells with subsequent acquisition of a mesenchymal phenotype leading to the production of a fibrotic ECM. Although abnormal vascular development and remodeling are known CDH traits, there is limited data on EndoMT in CDH-PH. The overall aim was to investigate how EndoMT contributes to CDH-PH by identifying cells undergoing EndoMT as noted by alpha smooth muscle actin (α-SMA) expression in human umbilical vein endothelial cells (HUVECs), and murine lung tissue utilizing the nitrofen model. The hypotheses were that EndoMT is increased in CDH endothelial cells and lung tissue and when compared to controls. HUVECs demonstrated a 1.1-fold increase in α-SMA expression (p=0.02), with a 0.7-fold increase in CD31 (p=NS). There was a 0.4-fold increase in α-SMA and 0.8-fold decrease in CD31 expressions in the nitrofen pup lungs when compared to controls. These results suggest EndoMT may contribute to the ECM remodeling seen in neonatal CDH-PH.

Introduction

Every 10 minutes in the United States, a baby is born with congenital diaphragmatic hernia (CDH) according to Shanmugam, et al. [1]. The incidence of CDH is estimated at 1 per 2,000 to 5,000 births [2]. CDH is an anatomic defect where the diaphragm fails to form completely and allows abdominal viscera to herniate into the thorax. CDH is a complex disease with multifactorial pathology, high morbidity, and mortality of 25-30% during the neonatal period [3]; morbidity and mortality largely results from the pulmonary hypertension (PH) and lung hypoplasia that are characteristic of CDH. PH is defined as sustained, supra-normal pulmonary arterial pressure that creates dysfunctional pulmonary circulation and suboptimal gas exchange with subsequent decreased oxygenation, ventilation, and/or cardiac function [3]. Patients with CDH have structurally and functionally abnormal pulmonary vessels that may contribute to PH [4]. Despite clinical advances in therapy, pulmonary hypertension secondary to CDH (CDH-PH) remains a major medical challenge in the management of patients with CDH postnatally.

Research shows extracellular matrix (ECM) thickening in the CDH pulmonary vasculature [5]. Thickening of the media and adventitia of pulmonary arteries creates a stiff ECM in CDH which decreases luminal diameter, increases resistance to blood flow, and decreases vascular compliance [6]. Therefore, a stiff pulmonary vascular ECM causes the pulmonary vessel to become a "lead pipe," reducing blood flow and responsiveness to anti-PH therapies. A major gap in knowledge is the nascence of the science on molecular drivers that promote pathogenic ECM remodeling in CDH-PH. One pathway of interest is endothelial-to-mesenchymal transition (EndoMT), which promotes abnormal pulmonary vascular ECM remodeling and drives PH in multiple adult and pediatric PH diseases; however, EndoMT has not been studied in CDH-PH [7]. The lack of EndoMT research in CDH-PH is likely due to difficulties in obtaining CDH lung tissue to study endothelial cells.

EndoMT features a progressive loss of native endothelial cell (EC) markers and acquisition of a mesenchymal cell phenotype with the production of a fibrotic ECM. During EndoMT, endothelial cells differentiate into mesenchymal-like cells characterized by induced α-SMA expression with a loss of endothelial cell markers and increased collagen deposition [8]. With EndoMT, there is downregulation of the endothelial-specific marker CD31, and upregulation of mesenchymal marker α-SMA [9]. Abnormal vascular development and ECM remodeling are CDH traits, but compelling data that decipher if EndoMT mechanistically contributes to CDH-PH have not yet been obtained. The overarching hypothesis is that EndoMT is increased in endothelial cells and CDH lung tissue when compared to controls. This hypothesis was tested to improve global knowledge of a potential underlying mechanism, EndoMT, that could be contributing to the ECM thickening seen in CDH-PH.

Materials and Methods

HUVECs

Endothelial dysfunction is a known feature of CDH-PH tissues [10]; differences in the endothelial response seen in CDH secondary to lung hypoplasia and organ compression may be responsible for differences in CDH-PH severity and postnatal treatment response. To address this, HUVECs have been investigated to understand the behavior of pulmonary vascular endothelial cells as a surrogate *ex vivo* model [11]. Briefly, HUVEC-based models have been used since the 1970s as a method to study vascular endothelium properties in conjunction with molecular mechanisms involved in endothelial cell function [11,12], which helped to glean insight into vascular biology by evaluating different proteins involved in angiogenesis [11]. HUVECs represent an abundant and non-invasive resource that may demonstrate endothelial dysfunction in neonates with CDH-PH. This well-established model was used to study endothelial cell pathophysiology in CDH-PH to help uncover inherent differences in EndoMT expression

in healthy controls and neonates with CDH-PH.

Gestational age-matched controls were compared with CDH HUVEC specimens that were previously obtained and were stored in our laboratory's HUVEC biobank. The study sample size of 16 (8 healthy control and 8 CDH) was estimated with a medium effect size hypothesized on a theoretical basis utilizing EndoMT studies from a non-CDH-PH population that showed a three-to-six-fold increase in EndoMT marker α-SMA and a one-fold decrease in CD31 expression in endothelial cells [13]. The independent *t*-test with a two-tailed α=0.05, β= 0.80 or 80%, and a 20% attrition rate, was used in the sample size estimate. HUVECs previously obtained from twin births were excluded from this study due to lack of generalizability to the CDH population as only six cases of CDH have been documented in twins [14]. HUVECs were cultured and placed in a four-well cell culture chamber with 50,000 cells per well. The HUVECs were then exposed to TGF-β, a known EndoMT promoter, for 24 hours. Primary antibodies Sigma mouse (A5228) for α-SMA and Abcam rabbit (Ab28364) for CD31 were used and diluted with PBS 1:200 for α-SMA and 1:100 for CD31. The secondary antibodies were goat anti-mouse green (A11001; AF488) for α-SMA and goat anti-rabbit red (A11012; AF594) for CD31 with a 1:200 dilution. The spatiotemporal expression of the EndoMT markers were examined by immunofluorescence utilizing the Leica DMi8 fluorescence microscope.

The use of a standardized and documented protocol for immunofluorescent analysis enhanced reproducibility of the findings. Previously collected HUVEC samples had endothelial cells isolated using a standardized protocol to decrease variability in endothelial cell isolation.

Nitrofen Murine Model

The well-established nitrofen-induced mouse model was used to investigate *in vivo* differences in EndoMT biomarkers between CDH and healthy control pups. This model,

which is widely used in CDH research, causes murine pups to develop a diaphragmatic defect and lung maldevelopment similar to that observed in human CDH. Due to the nearly uniform mortality by postnatal day one, this model was used to study the early development of CDH-PH and the contribution of EndoMT in its pathogenesis [15].

A total of 16 lung tissue samples (n=8 murine CDH and n=8 murine controls) were utilized to measure the distribution of α-SMA and CD31 in murine pup lung tissue. Post-mortem lung tissue samples obtained from mice with a nitrofen-induced CDH phenotype were evaluated for the extent of EndoMT presence and compared with control mouse pup lungs from pregnant dams who did not receive nitrofen. Briefly, CD1 pregnant dams were gavaged with 50 mg of nitrofen diluted in olive oil at embryonic day 8.5 (CDH group). Pregnant dams of both the control and CDH group underwent C-section at embryonic day 18.5 and pup lungs were harvested and processed utilizing the Leica ASP300S machine, embedded as whole organ mounts, and placed in paraffin blocks for preservation. When preparing lung tissue samples for assessment, orientation was controlled by placing the left lung on the left side of the cassette. The paraffin blocks were sectioned, placed on slides, de-paraffinized, and stained with the same antibodies utilized in the previously described HUVEC model to examine the spatiotemporal expression of EndoMT markers α-SMA and CD31 to determine the presence of EndoMT in nitrofen versus control murine lung tissue samples. Standardized and documented protocols for all murine experiments conducted enhanced reproducibility of the analysis and findings.

Immunofluorescence images of the HUVECs and murine lung tissues from CDH and control patients and pups, respectively, were taken on the Leica DMi8 microscope using 20x magnification and a standardized image size. To quantify the degree of α-SMA expression, images were analyzed utilizing Fiji software (version 12.32.18) to measure

the percent area of α-SMA green staining. The percent area of staining was normalized to the total number of cells in the slide image to quantify the areas of α-SMA and CD31 per cell. A t-test was performed using GraphPad Prism (version 9.0) for MAC, GraphPad Software, San Diego, California USA.

Results

When evaluating α-SMA expression in CDH versus control HUVECs, a 1.1-fold increase was noted in CDH HUVECs as shown in Figure 1. There was significance noted with a p value of 0.02 indicating a difference between α-SMA expression in CDH versus control HUVECs. Cohen's F indicated a large effect size (F=0.7) showing practical significance with a sample size of *n*=8 (GraphPad, Prism).

CD31 expression was analyzed using the same methods as α-SMA with the percent area of staining being normalized to the total number of cells in the slide image. Initially, a one-fold decrease in CD31 was projected as the cells underwent EndoMT. However, a 0.7-fold increase of CD31 in CDH cells was noted when compared to controls after being exposed for 24 hours to TGF-β. The p-value was not statistically significant (p=0.16). A posteriori effect size was calculated, and the sample size would need to be increased to a minimum of 12 subjects in order to potentially show statistical significance (GraphPad, Prism).

For the nitrofen murine model, α-SMA expression was noted to have a 0.4-fold increase in the nitrofen pup lungs versus control pup lungs as demonstrated in Figure 2 after normalizing α-SMA expression to the total number of endothelial cells. There was no statistical significance (p=0.57) noted between the nitrofen and control pup lungs. CD31 expression was also analyzed using the same methodology as α-SMA in the nitrofen versus control pup lungs. A 0.8-fold decrease in CD31 expression was noted in

nitrofen pup lungs when compared to controls (Figure 2). There was no statistical

significance between the two groups (p=0.2). Of note, there was a 6% attrition rate in the

control group dams: one mouse did not survive pregnancy due to an unknown medical

condition. The dams were replaced by two new female mice of breeding age. The

attrition rate for pups was also 6% in the control group as one mouse had pups excluded

from the study due to dysmorphism of unknown etiology.

Fluoroscopy images of HUVECs and murine lung tissue showed a visual

difference in expression (Figure 3).

Discussion

Investigation of EndoMT in CDH-PH is a novel concept. Prior research evaluated

prenatal imaging and genetic mechanisms of CDH-PH [3,4]. However, currently no

genetic markers or imaging can gauge how severe CDH-PH will be postnatally;

therefore, providing little guidance for management after birth. The main focus of the

present study was to explore pulmonary vascular remodeling as reflected by EndoMT

expression. The nitrofen murine model was not innovative, but the use of the HUVEC

model was deemed to be a strength of the study and represents a novel ex-vivo model

that may be useful for future research of vascular remodeling in fetuses and neonates

with CDH-PH.

Evidence of EndoMT was expected as increased α-SMA and decreased CD31

expression in CDH HUVECs and murine pup lung tissue. Comparison of CDH to control

HUVECs showed a 1.1-fold increase (p=0.02) in α-SMA expression and a statistically

insignificant 0.7-fold increase in CD31 expression. In the murine model, there was a 0.4-

fold increase in α-SMA expression and 0.8-fold decrease in CD31 expression, neither of

which was significantly different from controls. Marulanda, et al. [16] described similar

results in their preclinical model to those in the present study when staining CDH

pulmonary arteries for α-SMA; their images demonstrated increased pulmonary arterial smooth muscle proliferation and α-SMA when compared to controls. Utilizing the nitrofen murine model, Coleman and colleagues [17] demonstrated similar results showing increased α-SMA mRNA in nitrofen-induced pup lungs when compared to controls.

EndoMT has been linked to the pathogenesis of other fibrotic disorders, including pulmonary fibrosis and idiopathic portal hypertension [19]. While α-SMA is a known mesenchymal cell byproduct of EndoMT, type I collagen is also known to be produced when cells undergo EndoMT [19]. HUVEC RNA-sequencing in our lab looked at markers of EndoMT expression in HUVECs including α-SMA, CD31, and type 1 collagen. Even though α-SMA and CD31 were not the most robust, there were selected for this study because CD31 is an endothelial marker and α-SMA is a prominent mesenchymal marker. Future studies that evaluate the possible contribution of type I collagen to the thickened ECM in CDH-PH may yield evidence for a more robust EndoMT marker than the ones used in the present study.

Species based differences were suggested by the study findings. Expression of EndoMT markers was significant in the HUVEC CDH model but was not significant in the nitrofen murine CDH model. The advantages previously discussed offered by HUVECs as a noninvasive, ex-vivo research model could yield reproducible and valid findings of EndoMT expression in neonates. It seems clear from the findings of the present study that neither the nitrofen nor control murine models serve that purpose. The question is posed regarding the utility of the nitrofen murine model to evaluate EndoMT expression in a CDH model.

The nitrofen murine model has been used since the 1980s to study in-vivo mechanisms of CDH-PH. Since initiation of this model to date, there have been no major

discoveries that have led to clinical changes or major improvements in clinical outcomes. Perhaps, a different model would accelerate progress with breakthrough therapies in CDH-PH research that can have a clinical impact on critically ill neonates. Variations in the use of the nitrofen murine model are likely, even when guided by a standardized protocol, arising from nitrofen dosing, regurgitation of the herbicide, drug metabolism, and gavage time points.

Future research and clinical management of neonates with CDH-PH would benefit from investigating whether there is a relationship between EndoMT expression and clinical severity of illness. There was a wide range of expression of α-SMA and CD31 in the present study within both the HUVEC and murine models. The investigator compared the defects observed in the CDH nitrofen model for an association with the magnitude and direction of EndoMT biomarker expression. There appeared to be no systematic trend; for example, the mice with the most visible defects had different directions in magnitude of expression. Nonetheless, others may wish to explore in a systematic and adequately powered way the relationship between severity of illness and biomarker expression.

Identifying activation pathways for EndoMT, such as Notch signaling, would be beneficial in order to assist in decreasing the occurrence of EndoMT and fibrosis by inhibiting their activation. Activation of the Notch signaling pathway has been shown to be involved in the induction of EndoMT in animal models and various human pathological conditions [20]. Several Notch pathway inhibitors have been identified in cancer research and pharmacological agents are used to disrupt Notch transcription factors [21]. Expression of delta-like 4, a vascular endothelial ligand that activates Notch signaling to induce EndoMT [22], was noted to be upregulated in the postmortem human

CDH lung tissue samples when compared with age-matched postmortem lung tissue control samples. Discerning ways to reduce EndoMT with Notch activators and inhibitors could prove beneficial in decreasing ECM thickening in neonates with CDH-PH.

Aside from the conceptual limitations addressed above, a methodological limitation of the present study was the small sample sizes, leading to an underpowered study. Other methodological limitations include the possibility of errors in staining, even though standardized and documented protocols were used, and confounding effects from using the TGF-β promoter of EndoMT in the HUVEC model but not the nitrofen murine model.

The study findings yielded potentially useful information for the research community that can inform estimation of effect sizes and models to study EndoMT in neonates with CDH-PH. The strengths and limitations of the study and alternative approaches were suggested. More research is needed on the mechanisms of PH associated with CDH and biomarkers to inform early diagnostics and clinical management to improve patient outcomes.

Conclusion

The results of the study suggest EndoMT may contribute to CDH-PH as demonstrated by increased α-SMA in the HUVEC and murine models. The CD31 results were mixed and varied in direction and magnitude by model. Future studies are recommended to further elucidate and reproduce the findings.

References

1. Shanmugam H, Brunelli L, Botto LD, Krikov S, Feldkamp ML. Epidemiology and Prognosis of Congenital Diaphragmatic Hernia: A Population-Based Cohort Study in Utah. Birth Defects Res. 2017;109(18):1451-1459. doi:10.1002/bdr2.1106

2. AlFaleh K, Lee KS, Ramsey J, Nowaczyk M. Genetic considerations in recurrent congenital diaphragmatic hernia in two siblings. Annals of Saudi Medicine. 2006;26(5), 391–394. doi:10.5144/0256-4947.2006.391

3. Gupta VS, Harting MT. Congenital diaphragmatic hernia-associated pulmonary hypertension. Semin. Perinatol. 2020;44, 151167. PMID: 28641752

4. Mous DS, Buscop-van Kempen MJ, Wijnen R, Tibboel D, Rottier RJ. Changes in congenital diaphragmatic hernia associated pulmonary hypertension explain unresponsiveness to pharmacotherapy. Respiratory Research. 2017;18(1), 187. doi:10.1186/s12931-0170670-2

5. Monroe MN, Zhaorigetu S, Gupta VS, Jin D, Givan KD, Curylo AL, Olson SD, Cox CS, Segura A, Buja LM, Grande-Allen KJ, Harting MT. Extracellular vesicles influence the pulmonary arterial extracellular matrix in congenital diaphragmatic hernia. Pediatric pulmonology. 2020;55(9), 2402–2411. https://doi.org/10.1002/ppul.24914

6. Yamataka T, Puri P. Pulmonary artery structural changes in PH complicating congenital diaphragmatic hernia. J Pediatr Surg. 1997;32(3):387-390. PMID: 9093999

7. Li Y, Lui KO, Zhou B. Reassessing endothelial-to-mesenchymal transition in cardiovascular diseases. Nat Rev Cardiol. 2018;146, 873. PMID: 29748594

8. Spillman F, Miteva K, Pieske B, Tschope C, Van Linthout S. High Density Lipoproteins Reduce Endothelial to Mesenchymal Transition. American Heart Association. 2015. doi: 10.1161/ATVBAHA.115.305887

9. Zhang Y, Wu X, Zhang H, Li Z, Zhang Y, Zhang L, et al. Endothelial to mesenchymal transition contributes to arsenic-trioxide induced cardiac fibrosis. Scientific Reports. 2016;6, 33787. https://doi.org/10.1038/srep33787

10. Montalva L, Antounians PH, Zani A. Pulmonary hypertension secondary to congenital diaphragmatic hernia: factors and pathways involved in pulmonary vascular remodeling. Pediatrics Res. 2019;85, 754–768. PMID: 30780153

11. Medina-Leyte DJ, Domínguez-Pérez M, Mercado I, Villarreal-Molina MT, Jacobo Albavera L. Use of Human Umbilical Vein Endothelial Cells (HUVEC) as a Model to Study Cardiovascular Disease: A Review. Applied Sciences. 2020;10(3):938. https://doi.org/10.3390/app10030938

12. Baudin B, Bruneel A, Bosselut N, Vaubourdolle M. A protocol for isolation and culture of human umbilical vein endothelial cells. Nat. Protoc. 2007;2, 481–485. PMID: 17406610

13. Evrard S, Lecce L, Michealis K, Nomura-Kitabayashi A, Pandey G, Purushothaman KR, et al. Endothelial to mesenchymal transition is common in atherosclerotic lesions and is associated with plaque instability. Nature Communications. 2016;7, 11853. https://doi.org/10.1038/ncomms11853

14. Wang W, Pan W, Chen J, Xie W, Liu M, Wang J. Outcomes of Congenital Diaphragmatic Hernia in One of the Twins. Am J Perinatol. 2019;36(12):1304-1309. doi:10.1055/s-0038-1676830

15. Chiu PP. New Insights into Congenital–Diaphragmatic Hernia - A Surgeon's Introduction to CDH Animal Models. Frontiers Pediatrics. 2014;2:36. PMID: 2480904

16. Marulanda K, Tsihlis ND, McLean SE, Kibbe MR. Emerging antenatal therapies for congenital diaphragmatic hernia-induced pulmonary hypertension in preclinical models. Pediatr Res. 2021;89(7):1641-1649. doi:10.1038/s41390-020-01191-x

17. Coleman C, Zhao J, Gupta M, et al. Inhibition of vascular and epithelial differentiation in murine nitrofen-induced diaphragmatic hernia. Am J Physiol. 1998;274(4):L636-L646. doi:10.1152/ajplung.1998.274.4.L636

18. Evrard SM, Lecce L, Michelis KC, et al. Endothelial to mesenchymal transition is common in atherosclerotic lesions and is associated with plaque instability [published correction appears in Nat Commun. 2017 Feb 16;8:14710]. Nat Commun. 2016;7:11853. Published 2016 Jun 24. doi:10.1038/ncomms11853

19. Piera-Velazquez S, Li Z, Jimenez SA. Role of endothelial-mesenchymal transition (EndoMT) in the pathogenesis of fibrotic disorders. Am J Pathol. 2011;179(3):1074-1080. doi:10.1016/j.ajpath.2011.06.001

20. Piera-Velazquez, S., & Jimenez, S.A. Endothelial to Mesenchymal Transition: Role in Physiology and in the Pathogenesis of Human Diseases. Physiological Reviews. 2019; 99(2): 1281-1324. https://doi.org/10.1152/physrev.00021.2018

21. Lehal R, Zaric J, Vigolo M, et al. Pharmacological disruption of the Notch transcription factor complex. Proc Natl Acad Sci USA. 2020;117(28):16292-16301. doi:10.1073/pnas.1922606117

22. Zhou Q, Yang M, Lan H, Yu X. miR-30a negatively regulates TGF-β1-induced epithelial-mesenchymal transition and peritoneal fibrosis by targeting Snai1. Am J Pathol. 2013;183(3):808-819. doi:10.1016/j.ajpath.2013.05.019

Figure 1

α-SMA and CD31 Expression in Human Umbilical Vein Endothelial Cells

α-SMA Expression

*Dotted lines represent mean of control group (0.38), CDH group (0.57). p=0.02

*Left y-axis represents percent area of measurement for *α-SMA expression*

CD31 Expression

*Dotted lines represent mean of control group (0.2), CDH group (0.28). p=0.16

*Left y-axis represents percent area of measurement for *CD31 expression*
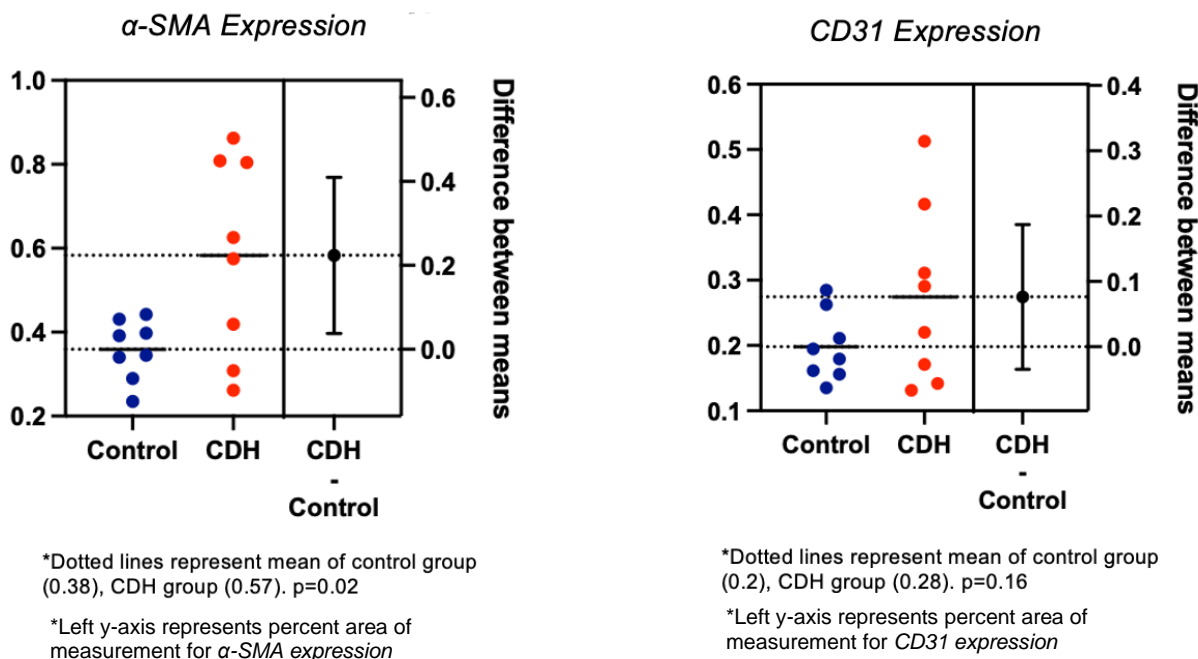
Figure 2

α-SMA and CD31 Expression in Murine Pup Lungs

α-SMA Expression

*Dotted lines represent mean of control group (0.13), CDH group (0.15). p=0.58

*Left y-axis represents percent area of measurement for *α-SMA expression*

CD31 Expression

*Dotted lines represent mean of control group (0.11), CDH group (0.14). p=0.21

*Left y-axis represents percent area of measurement for *CD31 expression*
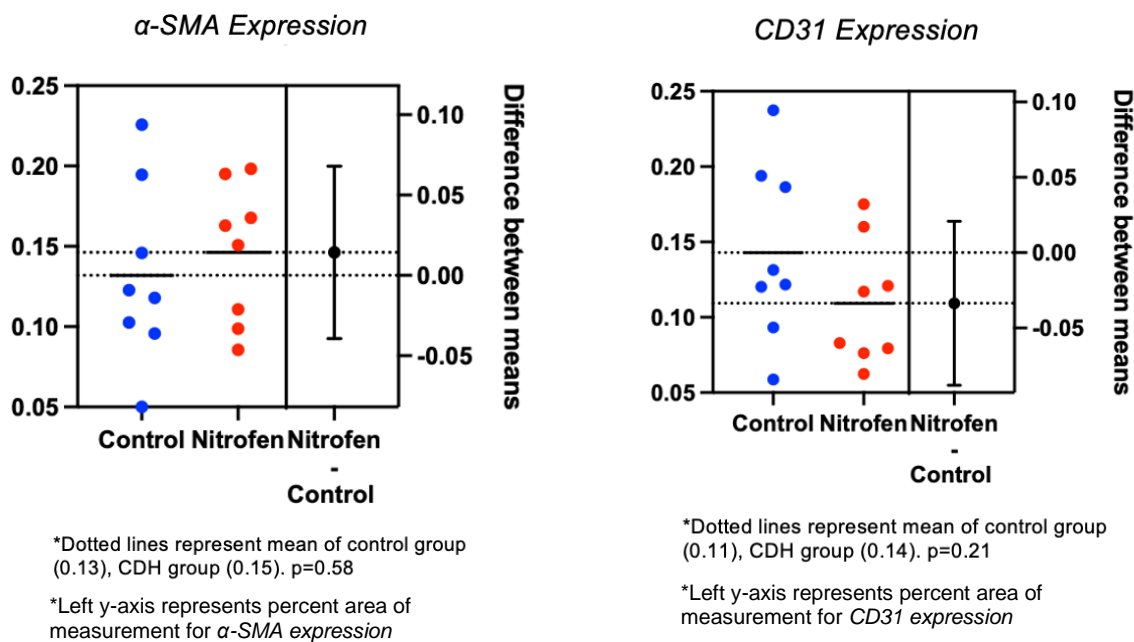
Figure 3

Fluoroscopy images of Human Umbilical Vein Endothelial Cells and Murine Pup Lung Tissue Stained for α-SMA, CD31, DAPI

a). b). c). d).
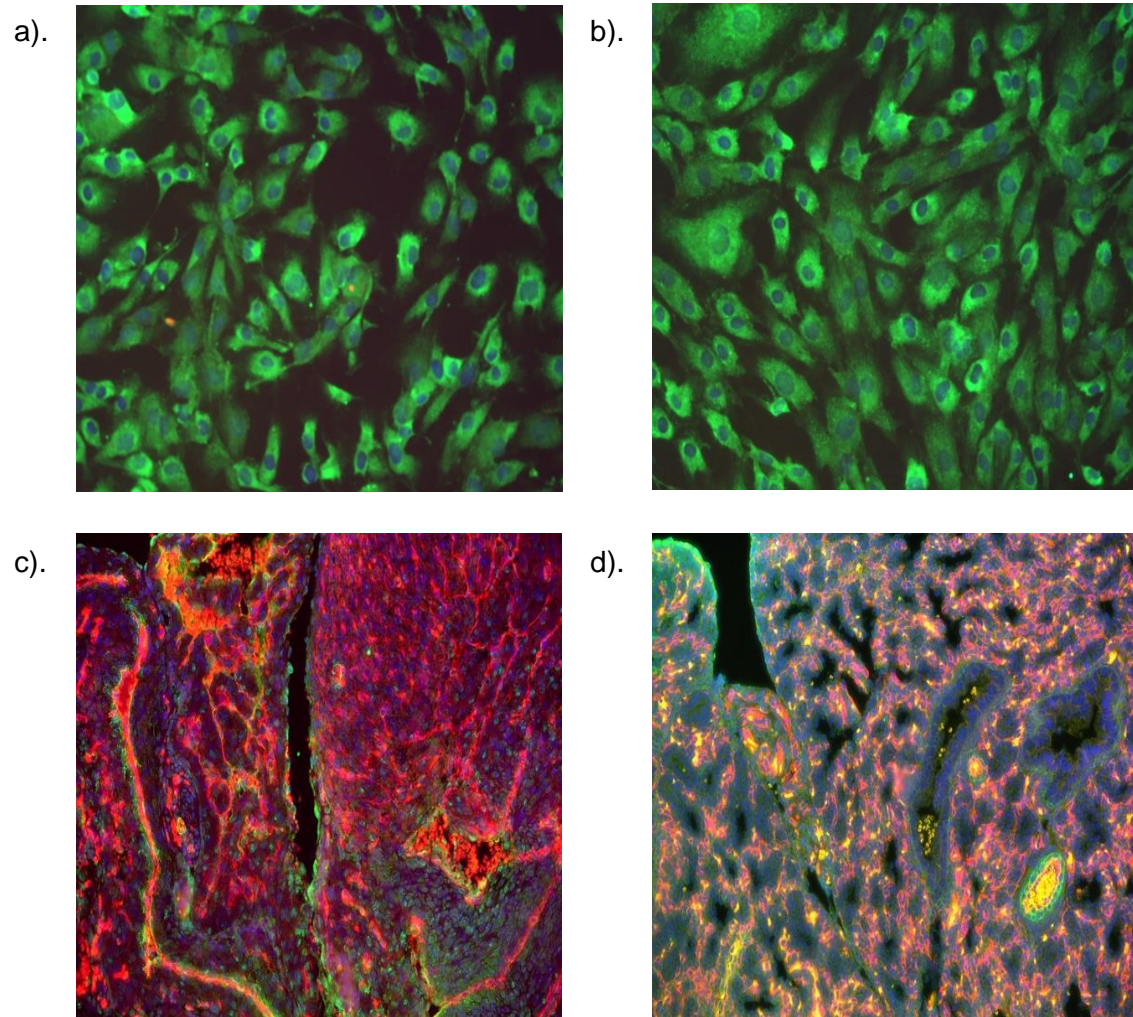
The panels represent fluoroscopy images of cells and tissue per the groups listed below. Panel b shows greater α-SMA expression than panel a (p=0.02). Panel d shows greater α-SMA expression compared to panel c. a). Control HUVECs exposed for 24hrs to TGF-β; b). CDH HUVECs exposed for 24h to TGF-β; c). Control pup lung; d). Nitrofen pup lung

Supplementary Material for Manuscript Submission

Table 1: HUVEC α-SMA Control Data

Control α-SMA	% Area	Number of Cells	Cells/%Area
Ctrl 1	22.12	50	0.44
Ctrl 2	51.58	178	0.29
Ctrl 3	69.67	202	0.34
Ctrl 4	53	123	0.43
Ctrl 5	52.46	223	0.24
Ctrl 6	58.93	173	0.34
Ctrl 7	77.55	195	0.40
Ctrl 8	36.41	93	0.39
			Mean= 0.36

Note. Ctrl=control: α-SMA= alpha smooth muscle actin

Table 2: HUVEC α-SMA CDH Data

CDH α-SMA	% Area	Number of Cells	Cells/%Area	Fold change	Increase/ Decrease
CDH 1	73.27	85	0.86	1.95	Increase
CDH 2	55.68	89	0.63	2.16	Increase
CDH 3	61.15	76	0.81	2.33	Increase
CDH 4	76.46	133	0.58	1.33	Increase
CDH 5	76.29	182	0.42	1.78	Increase
CDH 6	80.85	100	0.81	2.37	Increase
CDH 7	88.77	288	0.31	1.29	Decrease
CDH 8	56.32	215	0.26	1.49	Decrease
			Mean=0.59		
			Fold Change:	1.1-Fold	α-SMA Increase

Note. CDH=congenital diaphragmatic hernia: α-SMA= alpha smooth muscle actin

Table 3: HUVEC CD31 Control Data

Control CD31	% Area	Number of Cells	Cells/%Area
Ctrl 1	14.8	52	0.28
Ctrl 2	33.7	188	0.18
Ctrl 3	35	217	0.16
Ctrl 4	30.8	158	0.19
Ctrl 5	36	231	0.16
Ctrl 6	36.5	173	0.21
Ctrl 7	33.5	248	0.14
Ctrl 8	26	99	0.26
			Mean= 0.2

Note. Ctrl=control

Table 4: HUVEC CD31 Control Data

Note. CDH=congenital diaphragmatic hernia

CDH CD31	% Area	Number of Cells	Cells/%Area	Fold Change	Increase/ Decrease
CDH 1	25	86	0.29	1.02	Increase
CDH 2	27.7	89	0.31	1.74	Increase
CDH 3	40	78	0.51	3.18	Increase
CDH 4	20.7	146	0.14	1.37	Decrease
CDH 5	35	159	0.22	1.41	Increase
CDH 6	35.8	86	0.42	1.97	Increase
CDH 7	33.4	254	0.13	1.03	Decrease
CDH 8	36.1	211	0.17	1.54	Decrease
			Mean=0.27		
			Fold Change:	0.7-Fold	CD31 Increase

Table 5: Nitrofen Data Table Describing Pup Weights and Diaphragm Appearance

Right Uterine Horn	Pup Weight (mg)	Left Uterine Horn	Pup Weight (mg)	Pup Number	Diaphragm Defect
1	1074.4	8	1035.1	1	Thin membrane
2	1051.8	9	980.9	2	Thin membrane
3	1007.6	10	1072.5	3	Left side hole, thin membrane
4	1163.6	11	1149.6	4	Thin membrane
5	995.8	12	1041.4	5	Thin membrane
6	852.6	13	882.8	6	Thin membrane
7	1003.4			7	Thin membrane
				8	Thin membrane, ? hiatal hernia
				9	Thin membrane, ? hiatal hernia
				10	Right side hole, thin membrane
				11	Thin membrane
				12	Thin membrane
				13	Thin membrane

Table 6: Nitrofen Pup Data Table Lung Description Results

Pup Number	Lung Description	Results	Percent of Pups with Defect
1	Normal	13 thin membranes	100% thin membranes
2	Left lung smaller	1 Left defect	7% left defect
3	Left lung smaller	1 Left defect	7% left defect
4	Left lung smaller	2 Hiatal	15% hiatal hernias
5	Normal	4 Left lungs small	31% left lungs small
6	Normal		
7	Normal		
8	Normal		
9	Left lung smaller		
10	Normal		
11	Normal		
12	Normal		
13	Normal		

Table 7: Control Pup Data Table

Right Uterine Horn	Pup Weight (mg)	Left Uterine Horn	Pup Weight (mg)	Pup Number	Diaphragm Defect	Lung Description
1	1072.7	9	1375.3	1	None	Normal
2	1077.5	10	1286.7	2	None	Normal
3	983.3	11	970.9	3	None	Normal
4	1119.8	12	1047.1	4	None	Normal
5	1271.2			5	None	Normal
6	933.2			6	None	White appearance
7	842.9			7	None	Normal
8	874.3			8	None	White appearance
				9	None	Normal
				10	None	Normal
				11	None	Normal
				12	None	Normal

Table 8: Murine α-SMA Control Lung Tissue Data Table

Control α-SMA	% Area	Number of Cells	Cells/%Area
Ctrl 1	29.84	243	0.12
Ctrl 2	23.35	467	0.05
Ctrl 3	43.78	225	0.19
Ctrl 4	30.65	320	0.10
Ctrl 5	24.87	211	0.12
Ctrl 6	50.66	347	0.15
Ctrl 7	63.42	281	0.23
Ctrl 8	42.15	411	0.10
			Mean= 0.12

Note. Ctrl=control: α-SMA= alpha smooth muscle actin

Table 9: Murine α-SMA Nitrofen Lung Tissue Data Table

Nitrofen α-SMA	% Area	Number of Cells	Cells/%Area	Fold Change	Increase/ Decrease
Nitrofen 1	46.63	278	0.17	1.37	Increase
Nitrofen 2	47.04	312	0.15	3.02	Increase
Nitrofen 3	44.48	520	0.09	2.27	Decrease
Nitrofen 4	42.91	220	0.20	2.04	Increase
Nitrofen 5	43.99	397	0.11	0	None
Nitrofen 6	38.42	389	0.10	1.48	Decrease
Nitrofen 7	51.15	314	0.16	1.39	Decrease
Nitrofen 8	54.91	277	0.20	1.93	Increase
			Mean=0.15		
			Fold Change:	0.4-Fold	α-SMA Increase

Note. α-SMA= alpha smooth muscle actin

Table 10: Murine CD31 Control Lung Tissue Data Table

Control CD31	% Area	Number of Cells	Cells/%Area
Ctrl 1	29.59	243	0.12
Ctrl 2	27.47	467	0.06
Ctrl 3	41.95	225	0.19
Ctrl 4	38.49	320	0.12
Ctrl 5	50.11	211	0.24
Ctrl 6	45.58	347	0.13
Ctrl 7	54.48	281	0.19
Ctrl 8	38.32	411	0.09
			Mean= 0.14

Note. Ctrl=control

Table 11: Murine CD31 Nitrofen Lung Tissue Data Table

Nitrofen CD31	% Area	Number of Cells	Cells/%Area	Fold Change	Increase/ Decrease
Nitrofen 1	33.63	278	0.12	0	None
Nitrofen 2	49.95	312	0.16	2.72	Increase
Nitrofen 3	32.43	520	0.06	2.99	Decrease
Nitrofen 4	38.53	220	0.18	1.46	Increase
Nitrofen 5	31.55	397	0.08	2.99	Decrease
Nitrofen 6	29.68	389	0.08	1.72	Decrease
Nitrofen 7	36.79	314	0.12	1.65	Decrease
Nitrofen 8	22.99	277	0.08	1.12	Decrease
			Mean= 0.11		
			Fold Change:	0.8-Fold	CD31 Decrease

Statistical Analysis for HUVECs

Table 12: α-SMA Expression in Control versus CDH HUVECs using Cells per Percent Area

Control HUVECs	α-SMA Expression	CDH HUVECs	α-SMA Expression
Ctrl 1	0.44	CDH 1	0.86
Ctrl 2	0.29	CDH 2	0.63
Ctrl 3	0.34	CDH 3	0.81
Ctrl 4	0.43	CDH 4	0.58
Ctrl 5	0.24	CDH 5	0.42
Ctrl 6	0.34	CDH 6	0.81
Ctrl 7	0.40	CDH 7	0.31
Ctrl 8	0.39	CDH 8	0.26

Independent *t*-test (2- tailed), *t*=2.59, *df*= 14, *p*=0.02
Note. Ctrl=control: α-SMA= alpha smooth muscle actin: HUVECS=human umbilical vein endothelial cells: CDH= congenital diaphragmatic hernia

Table 13: CD31 Expression in Control versus CDH HUVECs using Cells per Percent Area

Control HUVECs	CD31 Expression	CDH HUVECs	CD31 Expression
Ctrl 1	0.28	CDH 1	0.29
Ctrl 2	0.18	CDH 2	0.31
Ctrl 3	0.16	CDH 3	0.51
Ctrl 4	0.19	CDH 4	0.14
Ctrl 5	0.16	CDH 5	0.22
Ctrl 6	0.21	CDH 6	0.42
Ctrl 7	0.14	CDH 7	0.13
Ctrl 8	0.26	CDH 8	0.17

Independent *t*-test (2- tailed), *t*=1.48, *df*= 14, *p*=0.16
Note. Ctrl=control: α-SMA= alpha smooth muscle actin: HUVECS=human umbilical vein endothelial cells: CDH= congenital diaphragmatic hernia

Statistical Analysis for Nitrofen Model

Table 14: α-SMA Expression in Nitrofen versus Control Pup Lungs using Cells per Percent Area

Control Pup Lungs	α-SMA Expression	Nitrofen Pup Lungs	α-SMA Expression
Ctrl 1	0.12	Nitrofen 1	0.17
Ctrl 2	0.05	Nitrofen 2	0.15
Ctrl 3	0.19	Nitrofen 3	0.09
Ctrl 4	0.10	Nitrofen 4	0.20
Ctrl 5	0.12	Nitrofen 5	0.11
Ctrl 6	0.15	Nitrofen 6	0.10
Ctrl 7	0.23	Nitrofen 7	0.16
Ctrl 8	0.10	Nitrofen 8	0.20

Independent *t*-test (2- tailed), *t*=0.57, *df*= 14, *p*=0.58
Note. Ctrl=control: α-SMA= alpha smooth muscle actin

Table 15: CD31 Expression in Nitrofen versus Control Pup Lungs using Cells per Percent Area

Control Pup Lungs	CD31 Expression	Nitrofen Pup Lungs	CD31 Expression
Ctrl 1	0.12	Nitrofen 1	0.12
Ctrl 2	0.06	Nitrofen 2	0.16
Ctrl 3	0.19	Nitrofen 3	0.06
Ctrl 4	0.12	Nitrofen 4	0.18
Ctrl 5	0.24	Nitrofen 5	0.08
Ctrl 6	0.13	Nitrofen 6	0.08
Ctrl 7	0.19	Nitrofen 7	0.12
Ctrl 8	0.09	Nitrofen 8	0.08

Independent *t*-test (2- tailed), *t*=1.32, *df*= 14, *p*=0.21
Note. Ctrl=control

Appendix A: Baylor College of Medicine Animal Welfare Committee Approval

June 28, 2022

Baylor College of Medicine
Office of Research
One Baylor Plaza, 600D
Houston, Texas 77030
Phone: (713) 798-6970
Fax: (713) 798-6990
Email: iacuc@bcm.edu

SUNDEEP KESWANI
BAYLOR COLLEGE OF MEDICINE
SURGERY: PEDIATRIC SURGERY DIV.

AN-6880: MOLECULAR MECHANISMS OF REGENERATIVE WOUND HEALING

APPROVAL VALID FROM June 28, 2022 thru June 27, 2025

Dear Dr. KESWANI

The animal care and use of your research protocol indicated above has been approved by the Institutional Animal Care and Use Committee of Baylor College of Medicine.

Baylor College of Medicine has an Animal Welfare Assurance approved by the Office of Laboratory Animal Welfare (OLAW), meeting the requirements of the Public Health Service Policy on Humane Care and Use of Laboratory Animals. The Assurance number is D16-00475.

As principal investigators of this research, you are required to provide a copy of the approved protocol and all subsequently approved amendments to each individual working on this project for their reference.

You will be notified should any U.S.D.A., Baylor College of Medicine, VAMC (if applicable) or other policies come into effect that would require you to amend your project.

Respectfully,

FREDERICK PEREIRA, PH.D., B.SC.
Institutional Animal Care and Use Committee

Appendix B: UT Health CPHS Exemption Letter

UTHealth
The University of Texas
Health Science Center at Houston

Committee for the Protection of Human Subjects

6410 Fannin Street, Suite 1100
Houston, Texas 77030

TO: Jamie Gilley
        Cizik School of Nursing

FROM: Sylvia Romo
        IRB Coordinator
        CPHS Office

DATE: June 18, 2022

RE: HSC-SN-22-0507 - *Endothelial to mesenchymal transition in human and murine models of congenital diaphragmatic hernia pulmonary hypertension*

Reference Number: 231294

Dear Jamie Gilley,

The Committee for the Protection of Human Subjects (CPHS) reviewed this submission and determined it does not meet the regulatory definition of human subjects research; no further review by CPHS is required.

Please confirm whether a Material Transfer Agreement/ Data Use Agreement will be required to transfer the samples from the Biobank at Baylor College of Medicine. For additional guidance and required forms please visit the Sponsored Projects Administration Website at **https://www.uth.edu/sponsored-projects-administration/tools-resources/forms-templates**

If you have any questions, please contact **Sylvia.Romo@uth.tmc.edu**

The submission in iRIS is now closed. Thank you.

Appendix C: Immunofluorescence Protocol for Cells (Revised)

<u>Assembly of Equipment and Supplies</u>

- Nonsterile gloves

- Four chamber well slides with CDH and control HUVECs fixed at 60,000 cells per chamber

- PBS solution

- Triton solution

- BSA solution

- Sigma mouse ASMA primary antibody A5228; 1:200 dilution

- Abcam rabbit CD31 primary antibody Ab28364; 1:100 dilution

- Goat anti-rabbit red CD31 secondary antibody A11012; AF594; 1:200 dilution

- Goat anti-mouse green ASMA secondary antibody A11001; AF488; 1:200 dilution

- DAPI mounting medium

- Slide coverslip

- Leica DMI-8 Fluoroscopy microscope

<u>Permeabilization</u>

If the target protein is intracellular, it is very important to permeabilize the cells.

1. Don nonsterile gloves. Incubate the samples for 10 min with PBS containing 0.1% Triton. Triton X-100 is the most popular detergent for improving the penetration of the antibody. However, it is not appropriate for membrane-associated antigens since it destroys membranes.

2. Wash cells in 300μL PBS three times for 5 mins each time.

Multicolor immunostaining

To examine the co-distribution of two (or more) different antigens in the same sample, use a double immunofluorescence procedure. This can be performed either simultaneously (in a mixture) or sequentially (one antigen after another).

Ensure you have antibodies for different species and their corresponding secondary antibodies. For example, rabbit antibody against antigen A, mouse antibody against antigen B.

Simultaneous incubation

1. Incubate cells with 300µL Daoko Antibody blocking solution for 30 min to block unspecific binding of the antibodies.
2. Incubate cells with both primary antibodies (Sigma mouse ASMA primary antibody A5228; 1:200 dilution in PBS. Abcam rabbit CD31 primary antibody Ab28364; 1:100 dilution in PBS) in a humidified chamber for 1 h at room temperature.
3. Decant the solution and wash the cells three times in 300µL PBS for each well, 5 min each wash.
4. Incubate cells with both secondary antibodies (Goat anti-rabbit red CD31 secondary antibody A11012; AF594; 1:200 dilution in PBS. Goat anti-mouse green ASMA secondary antibody A11001; AF488; 1:200 dilution in PBS) for 1 h at room temperature in the dark.
5. Decant the secondary antibody solution and wash three times with 300 µL PBS for 5 mins each in the dark.

Mounting

1. Mount coverslip with a drop of DAPI mounting medium.

2. Place coverslip to prevent drying and movement under microscope.

3. Store in dark at room temperature.

Reference

Abcam, 2021. Protocol obtained and modified for purposes of this study from

https://www.abcam.com/index.html?pageconfig=popular_protocols

HUVEC Slide Layout
50,000 cells per well; TGFb exposure for 24 hours

No TGFB Ctrl1	No TGFB CDH3	TGFB Ctrl1	TGFB CDH3

No TGFB Ctrl2	No TGFB CDH5	TGFB Ctrl2	TGFB CDH5

No TGFB Ctrl3	No TGFB CDH6	TGFB Ctrl3	TGFB CDH6

No TGFB Ctrl4	No TGFB CDH8	TGFB Ctrl4	TGFB CDH8

No TGFB Ctrl5	No TGFB CDH9	TGFB Ctrl5	TGFB CDH9

No TGFB Ctrl7	No TGFB CDH10	TGFB Ctrl7	TGFB CDH10

No TGFB Ctrl9	No TGFB CDH12	TGFB Ctrl9	TGFB CDH12

No TGFB Ctrl10	No TGFB CDH13	TGFB Ctrl10	TGFB CDH13

Negative Control

No TGFB Ctrl10	No TGFB CDH13	TGFB Ctrl10	TGFB CDH13

No TGFB Ctrl1	No TGFB CDH3	TGFB Ctrl1	TGFB CDH3

No TGFB Ctrl2	No TGFB CDH5	TGFB Ctrl2	TGFB CDH5

No TGFB Ctrl3	No TGFB CDH6	TGFB Ctrl3	TGFB CDH6

No TGFB Ctrl4	No TGFB CDH8	TGFB Ctrl4	TGFB CDH8

No TGFB Ctrl5	No TGFB CDH9	TGFB Ctrl5	TGFB CDH9

No TGFB Ctrl7	No TGFB CDH10	TGFB Ctrl7	TGFB CDH10

No TGFB Ctrl9	No TGFB CDH12	TGFB Ctrl9	TGFB CDH12

No TGFB Ctrl10	No TGFB CDH13	TGFB Ctrl10	TGFB CDH13

Negative Control

No TGFB Ctrl10	No TGFB CDH13	TGFB Ctrl10	TGFB CDH13

Appendix D: Nitrofen Mouse Model Protocol (Revised)

The Nitrofen Mouse Model Protocol was developed for the Laboratory for Regenerative Tissue Repair at Texas Children's Hospital and Baylor College of Medicine by Jamie Gilley, APRN, MSN, NNP-BC, Cizik School of Nursing PhD Student as part of her PhD coursework.

Nitrofen Gavage:

- CD1 mice aged 9-13 weeks (15-30 grams) will be used.

- Females (*n*=2 female/cage) at estrous stage will be caged with potent males (*n*=1 male per 2 females per cage) in the afternoon with the male separated the next morning.

- Vaginal plug or sperm the next morning will be day 0 gestation.

- At embryonic day 8.5 (E8.5) 50 mg of nitrofen will be dissolved in 0.5 ml of olive oil for the nitrofen group and gavaged to the mother per protocol (see Gavage protocol below). The 0.5 time point will be at 1200 noon indicating a half day.

Post Nitrofen:

- At *E18.5 days*, pregnant females' pups will be delivered via C-section immediately after the mother is euthanized utilizing carbon dioxide inhalation. Post C-section, pups will be marked by number, placed in a warm saline bath, then characteristic evaluation will be performed to include pup weight, any apparent physical abnormalities in the pup, and whether the pup was obtained from the left horn or right horn of uterus.
    - o The laboratory scale used for weights is a Mettler Toledo scale that is serviced annually in the Laboratory for Regenerative Tissue Repair per manufacturers recommendations.
    - o Weighing dishes are used for each pup with the scale zeroed/tared prior to weighing each individual pup.

- Postmortem autopsy will be performed on the pups to identify if a CDH phenotype is present. A CDH phenotype will be confirmed if a hole is present in the diaphragm. To investigate the diaphragms integrity, circumferential dissection will be done below the diaphragm to observe if a diaphragmatic hole is present. After circumferential dissection, the sternum will be cut open and the ribs cut away to reveal the bilateral lungs. After rib removal, care must be taken to remove the lungs intact from the thoracic cavity.

Protocol for lung paraffin sections in mouse pup lungs:

1. The thoracic cavity of the mouse pup will be opened, and the lungs identified. Identification of CDH phenotype will include a diaphragmatic hole, potential organ herniation, and lung hypoplasia, if present. Due to the small size of the mouse pups, lung hypoplasia will be difficult to examine.

2. The mouse pup lungs will be removed and placed in a plastic cassette (see Fixation below).

3. The tissue will then be formalin fixed paraffin embedded (FFPE) for later staining/analysis (see Mouse Pup Lung Tissue Preservation below).

Nitrofen Mouse Pup Lung Tissue Preservation:

1. Fixation:

- Tissue will be placed in a plastic cassette and placed in 10% neutral buffered formalin fixative.

    o 10% neutral buffered formalin is the universal fixative and will be used.

    o Tissue should be no thicker than a nickel (3-5mm) and should not be compressed by the cassette to prevent tissue damage.

    o Tissue should be no larger than a stamp.

- Fixative volume must be 20 times greater than the tissue volume. Ensure all parts of the specimen are submerged in the fixative solution.
- Fix tissue for 24 hrs in the formalin fixative.

2. Dehydration (done by machine in The Laboratory for Regenerative Tissue Repair):

- 70% alcohol (ETOH) used initially
- 2 changes of 95% ETOH
- 3 changes of 100% ETOH
- Process takes several hours

3. Clearing (done by machine in The Laboratory for Regenerative Tissue Repair):

- Xylene utilized for paraffin to take effect
- The de-alcoholization process moves alcohol out of tissues

4. Processing:

- Paraffin infiltration for 2-3 hrs. This process holds the intracellular structures in place.
- The sample is then embedded in paraffin with the flat side down. Care must be taken to embed every sample the same, so tissue orientation is accurate.

Gavage Protocol:

Supplies:

- o Gavage needle of appropriate size
    - ▪ Mice 24 gauge, 1.5 inches in length
- o 1 ml syringe
- o Nitrofen+olive oil mixture

Prepare Syringe:

- Draw up solution into the syringe

- o   Adult volume not to exceed 10-20 ml/kg of body weight
- Attach gavage needle to syringe

  - o   Preload needle and remove air bubbles (rodents cannot vomit or regurgitate)

  - o   The volume in syringe needs to account for hub loss

Orogastric Gavage of the Mouse:

- Grasp mouse gently but firmly at the scruff of the neck. The neck must be straight and midline to allow for the airway to be open.

- Measure the needle length to verify it is long enough to reach the corner of the mouth to the last rib. Mark needle hub if needed for the correct depth.

- Position the mouse with mouth facing up and towards the holder.

- Insert the gavage needle gently into the back of the mouth following the upper palate into the esophagus. If resistance is felt, stop as the needle may be in the trachea. Withdraw the needle immediately if you believe it is in malposition.

- Once the needle is completely advanced, introduce the syringe contents, count to three, then remove. This process helps with absorption and decreases the risk of aspiration.

  - o   Stop the procedure immediately if:

    - ▪   The mouse struggles intensely during fluid introduction

    - ▪   The mouse coughs

    - ▪   Fluid is expelled from the nose of the mouse

- Observe the animal for 5-10 minutes to monitor for signs of:

  - o   Ruffled fur

  - o   Hunched posture

  - o   Decreased activity

- o If you believe the fluid was introduced to the lungs, euthanize the mouse
  immediately
- Sanitize or sterilize gavage needle before and after use.
- Discard used syringe in sharps container.

References used to develop the Nitrofen Mouse Model:

Chui, P. (2014). New Insights into Congenital Diaphragmatic Hernia, a Surgeons

    Introduction to CDH Animal Models. *Frontiers.* doi: 10.3389/fped.2014.00036

Cilley, R. E., Zgleszewski, S. E., Krummel, T. M., & Chinoy, M. R. (1997). Nitrofen dose

    dependent gestational day-specific murine lung hypoplasia and left-sided

    diaphragmatic hernia. *The American journal of physiology.* 272(2 Pt 1), L362

    L371. https://doi.org/10.1152/ajplung.1997.272.2.L362

Grzenda, A., Shannon, J., Fisher, J., & Arkovitz, M. S. (2013). Timing and expression of

    the angiopoietin-1-Tie-2 pathway in murine lung development and congenital

    diaphragmatic hernia. Disease models & mechanisms, 6(1), 106–114.

    https://doi.org/10.1242/dmm.008821

Keijzer, R., Liu, J., Deimling, J., Tibboel, D., & Martin Post, M. (2000). Dual-Hit

    Hypothesis Explains Pulmonary Hypoplasia in the Nitrofen Model of Congenital

    Diaphragmatic *Hernia. Am J Pathol.* 156(4): 1299–1306.

Lath, N. R., Galambos, C., Rocha, A. B., Malek, M., Gittes, G. K., & Potoka, D. A. (2012).

    Defective pulmonary innervation and autonomic imbalance in congenital

    diaphragmatic hernia. American journal of physiology. *Lung cellular and*

    molecular physiology. 302(4),L390–L398.

Leinwand, M. J., Zhao, J., Tefft, J. D., Anderson, K. D., & Warburton, D. (2002). Murine

    nitrofen induced pulmonary hypoplasia does not involve induction of TGF-beta

    signaling. *Journal of pediatric surgery.* 37(8), 1123–1127.

    https://doi.org/10.1053/jpsu.2002.34456

Leinwand, M.J., Tefft, J.D., Zhao, J., Coleman, C., Anderson, K.D., & Warburton, D.

    (2002). Nitrofen inhibition of pulmonary growth and development occurs in the

    early embryonic mouse. *J Pediatr Surg.* 37(9):1263-1268.

    doi:10.1053/jpsu.2002.34978

Nakao, Y., & Ueki, R. (1987). Congenital Diaphragmatic Hernia Induced by Nitrofen in Mice and Rats; Characteristics as Animal Model and Pathogenetic Relationship between Diaphragmatic Hernia and Lung Hypoplasia. *Cong. Anom.* 27:397-417

Rhodes, J., Saxena, D., Zhang, G., Gittes, G.K., & Potoka, D.A. (2015). Defective parasympathetic innervation is associated with airway branching abnormalities in experimental CDH. *Am J Physiol Lung Cell Mol Physiol.* 309(2):L168-L174. doi:10.1152/ajplung.00299.2014

Sato, H., Murphy, P., Hajduk, P., Takayasu, H., Kitagawa, H., & Puri, P. (2009). Sonic hedgehog gene expression in nitrofen induced hypoplastic lungs in mice. *Pediatric surgery international.* 25(11), 967–971. https://doi.org/10.1007/s00383-009-2452-5

Shue, E., Wu, J., Schecter, S., & Miniati, D. (2013). Aberrant pulmonary lymphatic development in the nitrofen mouse model of congenital diaphragmatic hernia. *Journal of pediatric surgery.* 48(6), 1198–1204. https://doi.org/10.1016/j.jpedsurg.2013.03.013

Wu, C.S., Chen, C.M., & Chou, H.C. (2016).Pulmonary Hypoplasia Induced by Oligohydramnios: Findings from Animal Models and a Population-Based Study. *Pediatr Neonatol.* doi: S1875-9572(16)30062-6.

Appendix E: Immunohistochemistry Staining Protocol for Formalin-Fixed Paraffin-Embedded (FFPE) Lung Tissue (Revised)

<u>Assembly of Equipment and Supplies</u>

- Leica autostainer machine

- Slides to be used for experiment

- Deionized water

- Wash buffer

- Substrate buffer

- FLEX DAB solution

- Sub Chromo solution

- All containers in Leica autostainer are labeled (ex: xylene container labeled

  xylene)

- Sigma mouse ASMA primary antibody A5228; 1:200 dilution

- Abcam rabbit CD31 primary antibody Ab28364; 1:100 dilution

- Goat anti-rabbit red CD31 secondary antibody A11012; AF594; 1:200 dilution

- Goat anti-mouse green ASMA secondary antibody A11001; AF488; 1:200

  dilution

- Tris-buffered saline (TBS)

- 0.025% Triton X-100

- Blocking 10% normal serum

- Bovine serum albumin

- DAPI mounting medium

- Slide coverslip

- Leica DMI-8 Fluoroscopy microscope

Antigen Retrieval:

Step 1 – Baking

- Don nonsterile gloves. Bake slides for 45 minutes at 56 degrees Celsius

Step 2 - Leica autostainer for deparaffinization and rehydration (The Leica autostainer is serviced annually in the Laboratory for Regenerative Tissue Repair per manufacturers recommendations)

- Turn on deionized water line at 45-degree angle

- Loading station container should be dry

- Unloading stations should be filled with deionized water (Milli-Q water)

- Run DEPARR - NO OVEN program on Leica autostainer. Ensure lids from the stations are removed prior to starting program.

Step 3 - PT Link (antigen retrieval)

- If needed, replace fluid after ~4 runs using 30 mL (entire bottle) of 50x solution mixed with 1470 mL deionized water
    - o Reset bulk fluid warning in Administrator drop down menu

- Pre-heat by clicking Run, and machine will take about 20 minutes to get to 75°C
    - o Once at 75°C, click Run again to run actual program with the low pH solution

- Take slides out soon after program ends and click Done in software
    - o Okay to leave slides in deionized water for ~1 day before staining

Staining Protocol:

- Blot the water with tissue paper taking care not to touch the lung tissue. Place a square around the lung tissue with a hydrophobic pen.

- Wash the slides 2x5 min in PBS with gentle agitation. Apply 25µL per section or 50µL per slide.

- Block in Daoko antibody diluent for 15 minutes at room temperature.

- Drain slides for a few seconds (do not rinse) and wipe around the sections with tissue paper

- Apply primary antibodies diluted Daoko antibody diluent. Sigma mouse ASMA primary antibody A5228; 1:200 dilution. Abcam rabbit CD31 primary antibody Ab28364; 1:100 dilution. Apply 25µL per section or 50µL per slide.

- Incubate overnight at 4°C.

- Rinse 2x5 min PBS with gentle agitation.

- Apply conjugated secondary antibody to the slide diluted in Daoko antibody diluent. Goat anti-rabbit red CD31 secondary antibody A11012; AF594; 1:200 dilution. Goat anti-mouse green ASMA secondary antibody A11001; AF488; 1:200 dilution. Apply 25µL per section or 50µL per slide.

- Incubate for 1 h at room temperature in the dark.

- Rinse 3x for 5 min with PBS in the dark.

- Mount using compatible DAPI and add coverslip.

- Store in a dark place to preserve fluorescence.

Interpreting Results:

- Increased α-SMA and decreased CD31 will be evaluated by microscopy to determine the presence of EndoMT expression and will be compared to control samples. Scientific significance will be noted by a threefold or greater increase in α-SMA expression and one-fold decrease in CD31 in CDH samples versus controls.

Reference

Abcam, 2021. Protocol obtained and modified for purposes of this study from

https://www.abcam.com/index.html?pageconfig=popular_protocols

Appendix F: IFC Analysis in Fiji Protocol (Revised)

IFC Analysis in Fiji:

1. Open the Fiji application and choose the image to be evaluated.

2. Select image-color-split channels-select channel to be used (green for ASMA, red for CD31 measurement).

3. Select image-adjust-threshold-analyze using auto threshold function for standardization.

4. Select analyze-set measurements-area-mean grey value-area fraction-limit to threshold- display label.

5. Select analyze-measure-document % area of the image.

Cell Count Analysis in Fiji:

1. Open the Fiji application and choose the image to be evaluated.

2. Select image-color-split channels-select blue channel to be used for cell count (DAPI staining).

3. Select image-adjust-threshold-analyze using auto threshold function for standardization.

4. Select analyze-analyze particles-(see screen shot below for settings)- document cell count number.
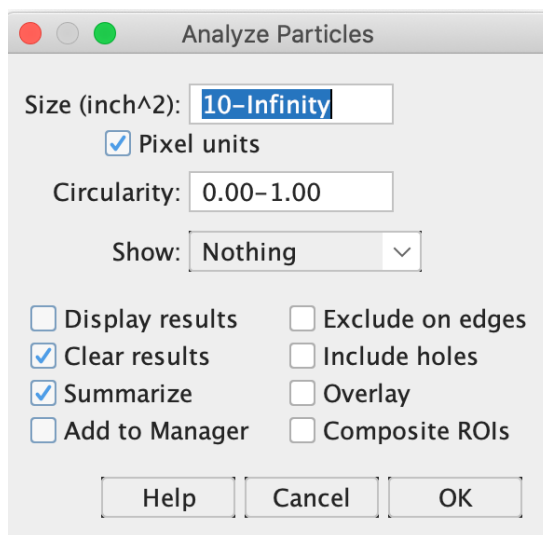
CURRICULUM VITAE
Jamie Gilley, PhD, APRN, MSN, NNP-BC

EDUCATION:

University of Texas, Health Science Center Cizik School of Nursing, Houston, Texas	2023	PhD	Nursing
University of Texas Medical Branch, Galveston, Texas	2012	MSN	Nursing
Texas A&M University, Corpus Christi, Texas	2007	BSN	Nursing

PROFESSIONAL POSITIONS:

Texas Children's Hospital,   2015-present
Houston, Texas
    Neonatal Nurse Practitioner

Rady Children's Hospital,   2013-2020
San Diego, California
    Neonatal Nurse Practitioner

Sharp Mary Birch Hospital,   2009-2012
San Diego, California
    Registered Nurse

Sacred Heart Hospital   2008-2009
Pensacola, Florida
    Registered Nurse

Driscoll Children's Hospital   2007-2008
Corpus Christi, Texas
    Registered Nurse

PROFESSIONAL MEMBERSHIPS:

Sigma Theta Tau International Honor Society for Nursing   2007-present

California Association of Nurse Practitioners   2011-2015
    San Diego, North Chapter

National Association Neonatal Nurses   2012-present

American Nurses Association, Texas Nurses Association   2020-present
Curriculum Vitae

JAMIE GILLEY
Page 2

PROFESSIONAL MEMBERSHIPS (Cont'd):

Southern Nursing Research Society   2022-present

PUBLICATIONS

Singampalli KL, Balaji S, Wang X, Parikh UM, Kaul A, Gilley J, Birla RK, Bollyky PL, Keswani SG. The Role of an IL-10/Hyaluronan Axis in Dermal Wound Healing. Front Cell Dev Biol. 2020; 8:636. PMID: 32850791.

Swanson LE, Gilley J, Masand P, Gowda S. Use of Laryngeal Mask Airway as a Bridge to Extracorporeal Membrane Oxygenation in a Neonate with Undiagnosed Tracheal Stenosis. Neonatal. 2020 October; 1(1):01. doi: 10.35702/NEO.10001.

Short WD, Wang X, Li H, Yu L, Kaul A, Calderon GA, Gilley J, Bollyky PL, Balaji S, Keswani SG. Interleukin-10 Producing T Lymphocytes Attenuate Dermal Scarring. Ann Surg. 2021. 10 01; 274(4):627-636. PMID: 34506318.

Olutoye II OO, Short WD, Gilley J, Hammond II JD, Belfort MA, Lee TC, King A, Espinoza J, Joyeux L, Lingappan K, Gleghorn JP, Keswani SG. The Cellular and Molecular Effects of Fetoscopic Endoluminal Tracheal Occlusion in Congenital Diaphragmatic Hernia. Front Pediatr.2022;10:925106. PMCID: PMC9294219.

Gilley, J. L., Holmes, A., Sims, E., Hanneman, S. K. (2022). Pulmonary embolism: Surveillance is key. American Nurse Journal, 17(3), 6-12. [IF = 2.22]

OTHER

Fernandes, CJ., Olutoye, O., Keswani, SK., Gilley, J, Lee, T., et. al. (2017). Acute Management of Congenital Diaphragmatic Hernia Evidenced Based Guideline. Evidenced Based Outcomes Center. TCH CDH Management Protocol

Prats, GP, Gilley, J, Rhee, C. (2017, 2018, 2019, 2020, 2021, 2022, 2023). Congenital Diaphragmatic Hernia. Fernandes, C (Ed. 25, 26, 27, 28, 29, 30), Baylor College of Medicine Neonatal Guidelines. Houston, TX. Guidelines for Acute Care of the Neonate.

Prats, GP, Gilley, J, Rhee, C. (2018, 2019, 2020, 2021, 2022, 2023). Neonatal ECMO. Fernandes, C (Ed. 26, 27, 28, 29, 30), Baylor College of Medicine Neonatal Guidelines. Houston, TX. Guidelines for Acute Care of the Neonate.

Curriculum Vitae
JAMIE GILLEY
Page 3

PRESENTATIONS:

Podium

      Gilley, J., Walker, S., Olutoye II, OO., Liu, H., & Keswani, S. (2022, February). The use of human umbilical vein endothelial cells as an ex vivo model in CDH-PH. Southern Nursing Research Society: Top 10 Student Podium Presentation. Podium presenter at the Southern Nursing Research Society Conference in New Orleans, LA.

      Gilley, J., Walker, S., Olutoye II, OO., Liu, H., & Keswani, S. (2022, April).The Role of Endothelial to Mesenchymal Transition in Congenital Diaphragmatic Hernia PH. Podium Presenter at the Congenital Diaphragmatic Hernia International Conference in Glasgow, Scotland.

      Gilley, J. (2022, Novemeber). The use of human umbilical vein endothelial cells as an ex vivo model in Congenital Diaphragmatic Hernia PH. Podium Presenter and Elevator Speech at UT Health Cizik School of Nursing Scholars Day.

Poster

      Gilley, J., Walker, S., Liu, H., & Keswani, S. (2021, February). Endothelial to Mesenchymal Transition in Congenital Diaphragmatic Hernia PH. Virtual poster presentation for Academic Surgical Congress.

      Gilley, J., Walker, S., Liu, H., & Keswani, S. (2021, April). The Potential Role of Endothelial to Mesenchymal Transition in Congenital Diaphragmatic Hernia PH. Virtual Poster Presentation at the Texas Childrens Hospital Advanced Practice Provider Conference.

      Gilley, J., Walker, S., Liu, H., & Keswani, S. (2021, May). The role of Endothelial to Mesenchymal Transition in Congenital Diaphragmatic Hernia PH. Virtual Poster Presentation at the Back to Science Symposium at Houston Methodist.

      Gilley, J., Walker, S., Olutoye II, OO., Liu, H., & Keswani, S. (2022, May). Human Umbilical Vein Endothelial Cells as an Ex Vivo Model in Congenital Diaphragmatic Hernia PH. Virtual Poster Presentation at the Texas Childrens Hospital Advanced Practice Provider Conference.

      Gilley, J., Rhee, C., Garcia-Prats, J., Mitchelll, A., Vogel, A., & King, A. (2022, September). Admission Central Line Placement in Infants Born with Congenital Diaphragmatic Hernia. Poster Presentation at the National Association of Neonatal Nurses Conference in Las Vegas, NV.

Curriculum Vitae
JAMIE GILLEY
Page 4

AWARDS AND RECOGNITION:

2002	Scholarship, Koch Industries ($2000).
2002	Scholarship, Padre Isles Country Club ($2000).
2007	Peer-nominated student commencement speaker.
2019	Rising Star Award, Baylor College of Medicine, Section of Neonatology.
2021	UT Health James A. Baker Transformation and Hope Scholarship ($3500).
2022	Texas Children's Hospital APRN of the Year.
2022	SNRS Third Place Student Presenter.
2022	Good Samaritan Excellence in Nursing in Houston, Bronze Award.